



Sr-Nd-Pb-Hf Isotope Results from ODP Leg 187: Evidence for Mantle Dynamics of the Australian-Antarctic Discordance and Origin of the Indian MORB Source

Pamela D. Kempton

*NERC Isotope Geosciences Laboratory, Kingsley Dunham Centre, Keyworth, UK, NG12 5GG
(p.kempton@nigl.nerc.ac.uk)*

Julian A. Pearce

Department of Earth Sciences, University of Cardiff, UK, CF10 3YE (pearceja@cardif.ac.uk)

Tiffany L. Barry

NERC Isotope Geosciences Laboratory, Kingsley Dunham Centre, Keyworth, UK, NG12 5GG (tbarry@bgs.ac.uk)

J. Godfrey Fitton

Grant Institute, University of Edinburgh, Edinburgh, UK, EH9 3JW (gfitton@glg.ed.ac.uk)

Charles Langmuir

Lamont-Doherty Geological Observatory and Department of Geological Sciences of Columbia University, Palisades, New York 10964, USA (langmuir@ldeo.columbia.edu)

David M. Christie

College of Oceanic and Atmospheric Sciences, Oregon State University, Oceanography Administration Building 104, Corvallis, Oregon 97331, USA (dchristie@oce.orst.edu)

[1] New high precision PIMMS Hf and Pb isotope data for 14–28 Ma basalts recovered during ODP Leg 187 are compared with zero-age dredge samples from the Australian-Antarctic Discordance (AAD). These new data show that combined Nd-Hf isotope systematics can be used as an effective discriminant between Indian and Pacific MORB source mantle domains. In particular, Indian mantle is displaced to lower ϵ_{Nd} and higher ϵ_{Hf} ratios compared to Pacific mantle. As with Pb isotope plots, there is almost no overlap between the two mantle types in Nd-Hf isotope space. On the basis of our new Nd-Hf isotope data, we demonstrate that Pacific MORB-source mantle was present near the eastern margin of the AAD from as early as 28 Ma, its boundary with Indian MORB-source mantle coinciding with the eastern edge of a basin-wide arcuate depth anomaly that is centered on the AAD. This observation rules out models requiring rapid migration of Pacific MORB mantle into the Indian Ocean basin since separation of Australia from Antarctica. Although temporal variations in isotopic composition can be discerned relative to the fracture zone boundary of the modern AAD at 127°E, the distribution of different compositional groups appears to have remained much the same relative to the position of the residual depth anomaly for the past 30 m.y. Thus significant lateral flow of mantle along the ridge axis toward the interface appears unlikely. Instead, the dynamics that maintain both the residual depth anomaly and the isotopic boundary between Indian and Pacific mantle are due to eastward migration of the Australian and Antarctic plates over a stagnated, but slowly upwelling, slab oriented roughly orthogonal to the ridge axis. Temporal and spatial variations in the compositions of Indian MORB basalts within the AAD can be explained by progressive displacement of shallower Indian MORB-source mantle by deeper mantle having a higher ϵ_{Hf} composition ascending ahead of the upwelling slab. Models for the origin of the distinctive composition of the Indian MORB-source based on recycling of a

heterogeneous enriched component that consist of ancient altered ocean crust plus <10% pelagic sediment are inconsistent with Nd-Hf isotope systematics. Instead, the data can be explained by a model in which Indian mantle includes a significant proportion of material that was processed in the mantle wedge above a subduction zone and was subsequently mixed back into unprocessed upper mantle.

Components: 17,321 words, 15 figures, 4 tables.

Keywords: Australian-Antarctic Discordance; Hf isotopes; Pb isotopes; Indian and Pacific MORB; subduction modified mantle; Ocean Drilling Program.

Index Terms: 1025 Geochemistry: Composition of the mantle; 1040 Geochemistry: Isotopic composition/chemistry; 8120 Tectonophysics: Dynamics of lithosphere and mantle—general; 9340 Information Related to Geographic Region: Indian Ocean.

Received 28 January 2002; **Revised** 20 May 2002; **Accepted** 29 May 2002; **Published** 17 December 2002.

Kempton, P. D., J. A. Pearce, T. L. Barry, J. G. Fitton, C. Langmuir, and D. M. Christie, Sr-Nd-Pb-Hf Isotope Results from ODP Leg 187: Evidence for Mantle Dynamics of the Australian-Antarctic Discordance and Origin of the Indian MORB Source, *Geochem. Geophys. Geosyst.*, 3(12), 1074, doi:10.1029/2002GC000320, 2002.

1. Introduction

[2] The Australian-Antarctic Discordance (AAD) is an unusually deep (4–5 km) region of the global mid-oceanic spreading system centred on the Southeast Indian Ridge (SEIR) between Australia and Antarctica (120° to 128°E). It is characterized by rough topography, long and closely spaced transforms, regional gravity lows, low magnetic anomaly amplitudes and multiple episodes of ridge propagation [Weissel and Hayes, 1974; Anderson *et al.*, 1980; Sempéré *et al.*, 1991; Palmer *et al.*, 1993]. Its anomalous depth is thought to reflect the presence of both unusually cold, possibly downwelling mantle [Marks *et al.*, 1991; Kuo, 1993] and thin crust [Forsyth *et al.*, 1987; Christie *et al.*, 1998]. The topographic expression of the depth anomaly forms a west-pointing V-shape, which cuts across the major fracture zones of the eastern AAD (Figure 1a) and implies that the depth anomaly has migrated westward at a long-term rate of ~15 mm/yr [Christie *et al.*, 1998].

[3] The AAD also encompasses an unusually sharp compositional boundary between Pacific MORB-source mantle (hereafter referred to as Pacific mantle) and Indian MORB-source mantle (Indian mantle) isotopic domains [Klein *et al.*, 1988; Pyle *et al.*, 1992]. In general, Pacific MORBs have lower $^{87}\text{Sr}/^{86}\text{Sr}$ for a given $^{143}\text{Nd}/^{144}\text{Nd}$ and lower $^{208}\text{Pb}/^{204}\text{Pb}$ for a given $^{206}\text{Pb}/^{204}\text{Pb}$ than Indian

MORBs [Rehkämper and Hofmann, 1997, and references therein]. The sharpness of the boundary between Indian and Pacific mantle, as expressed in the composition of seafloor lavas, suggests that Indian mantle presently abuts Pacific mantle beneath the AAD, with little or no intermingling [Pyle *et al.*, 1995; Christie *et al.*, 1998]. However, off-axis sampling within the AAD suggests that the isotopic boundary has migrated westward into and across the easternmost segment of the AAD at a rate of 25–40 mm/yr, at least over the last 3–4 Ma [Pyle *et al.*, 1995]. Thus the topographic expression of the AAD appears to have migrated at a different rate from the isotopic mantle domain boundary. Christie *et al.* [1998] proposed two competing hypotheses to explain this. Either the isotopic boundary migration is a localized perturbation of a geochemical feature associated with the depth anomaly since the basin opened (i.e., “slow” migration) or the migration is a longer-lived phenomenon that has only recently brought Pacific mantle beneath the AAD (i.e., “rapid” migration).

[4] Lanyon *et al.* [1995] identified Indian MORB on 36 Ma seafloor northeast of the current AAD (Dredge D10) and Pyle *et al.* [1995] identified Indian MORB-like crust as far east as 147°E (~64 Ma crust at ODP Site 280A; see Figure 1a), concluding that the current location of the isotopic boundary within the discordance is essentially coincidental. Similarly, Christie *et al.* [1998] con-

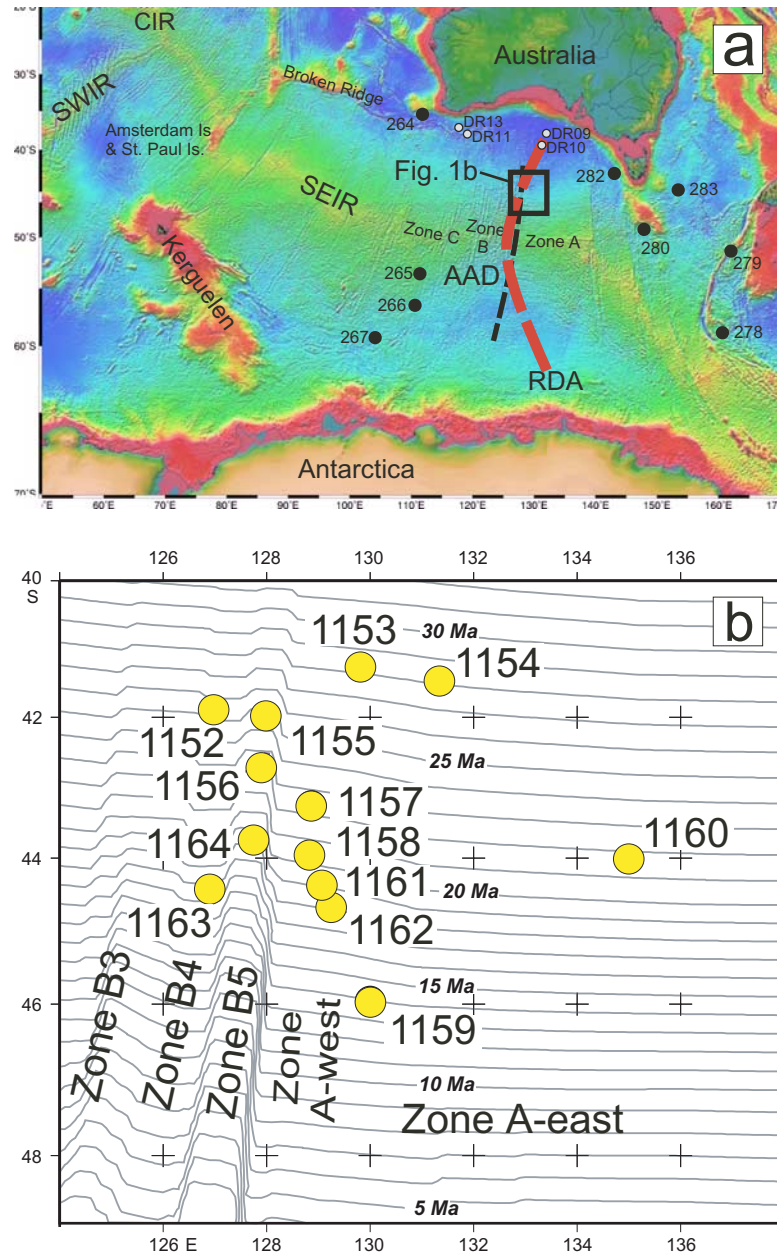


Figure 1. (a) Color shaded relief map of modelled topography of the Indian Ocean (modified from *Smith and Sandwell [1997]*). Approximate locations of Zones A, B and C within the AAD are shown; black dashed line is the trace of the 127°E fracture zone boundary between Zones A and B. SEIR = Southeast Indian Ridge. SWIR = Southwest Indian Ridge. CIR = Central Indian Ridge. Small black dots indicate the locations of older DSDP drill sites in the region; small grey dots are locations of dredge sites described by *Lanyon et al. [1995]*. Black square denotes location of Leg 187. Red dashed line (labeled RDA) is the approximate trace of the negative residual depth anomaly, i.e., areas where the depth is greater than predicted (from *Marks et al. [1990]*). (b) Map of the AAD showing the locations of Leg 187 drill sites (yellow circles) in relation to 1 m.y. isochrons (grey lines). Transform boundaries (such as between Zones B4 and B5 or Zones B5 and A) appear as deflections of the isochrons (figure modified from *Christie et al. [2001]*).

cluded that there was “limited support” for the rapid migration model, based on 0–7 Ma basalts dredged off-axis from the AAD. However, *Zhang et al. [1999]* argue that Pacific mantle was present

beneath eastern Gondwana prior to the eastward propagation of the SEIR, because 55–14 Ma basalts from southeastern Australia require a Pacific mantle-like isotopic component in their

source region. The purpose of ODP Leg 187 was to test these alternative models for the geodynamic evolution of the boundary between Indian and Pacific mantle by drilling 14–28 Ma oceanic crust in the vicinity of the residual depth anomaly (Figure 1a).

[5] Although lead isotope covariations easily distinguish young, on-axis MORB glasses of Indian and Pacific mantle origin [Hart, 1984; Hamelin and Allègre, 1985], it was unknown, prior to the analysis of the Leg 187 samples, whether this geochemical discriminant would be equally effective at locating the compositional boundary when applied to older, off-axis basalts. This is because the low concentration of Pb (0.3 ppm) in average N-MORB [Yang *et al.*, 1998; Mahoney *et al.*, 1998] and the extreme mobility of Pb and U in aqueous fluids [Kelly *et al.*, 2001] combine to modify both trace element and isotopic ratios, making age correction difficult. The ambiguous Pb isotope data for 47–69 Ma rocks from the South Tasman Rise provide a case in point. As stated by Pyle *et al.* [1995], whether these rocks are classified as Indian or Pacific depends on “the criteria used to define these upper mantle reservoirs.”

[6] We have therefore investigated the application of Nd-Hf isotope systematics as an alternative method of distinguishing between basalts derived from Indian versus Pacific MORB-source mantle. Pearce *et al.* [1999] synthesised the small amount of published data for Indian and Pacific MORBs, together with new data from arc and back arc rocks from the Western Pacific region, and suggested that Hf-Nd isotope space may be almost as effective as Pb isotope space in discriminating between Indian and Pacific mantle domains, while being less sensitive to alteration. Here we examine further this geochemical discrimination, its possible cause, and its implications for mantle dynamics within the AAD.

2. Background to Leg 187 Drilling

[7] Weissel and Hayes [1971] divided the SEIR south of Australia into three distinct zones based on seafloor topography (Figure 1a): Zone A (east of the AAD), Zone B (the AAD itself), and Zone C (west of the AAD). The axial morphology of Zone A is

similar to that of a fast spreading ridge like the East Pacific Rise, whereas the segmentation characteristics and axial topography of Zone B more closely resemble those of the slower spreading mid-Atlantic Ridge [West *et al.*, 1994]. Spreading rates are relatively constant along the SEIR (~ 74 mm/yr) [Weissel and Hayes, 1971] and therefore do not account for the large regional variations in ridge morphology.

[8] As the present locus of the AAD, Zone B has been further subdivided into five segments that are bounded by alternating north- and south-offset sections of the spreading center; from west to east these are referred to as Zones B1 to B5 [Vogt *et al.*, 1984]. The depth anomaly reaches a maximum of 1 km greater than average ridge depths in the center of the AAD in Zone B3 ($\sim 124^\circ\text{E}$), whereas the negative geoid anomaly is centred on the ridge axis in Zone B4 ($\sim 125^\circ\text{E}$) [Marsh *et al.*, 1986]. Today the isotopic boundary between Pacific and Indian mantle isotopic domains is located within Zone B5, ~ 100 km west of the province-bounding fracture zone at 127°E [Pyle *et al.*, 1992]. In the following sections we extend the on-axis zone designations to the Leg 187 drills sites. We emphasise that this is merely for convenience, intended to denote relative geographic position. It does not imply a particular mantle domain type in the off-axis setting, as neither the isotopic boundary, nor the center of the geoid anomaly, has remain fixed relative to the zone designations over time.

3. Summary of Leg 187 Drill Sites and Sample Selection

[9] Leg 187 drilled 23 different holes at 13 sites and recovered 137 m of core [Christie *et al.*, 2001]. The locations of the Leg 187 drill sites are shown in Figure 1b relative to seafloor isochrons. Sites 1153 and 1154 are located on the oldest crust drilled (~ 28 Ma) and Site 1159 on the youngest crust (14 Ma). Sites 1152 and 1163 are located in what is the off-axis equivalent of Zone B4 today. Sites 1155, 1156, and 1164 are located in Zone B5. All other sites are located in Zone A. Sites 1153, 1157, 1158, 1161, and 1162 form a N-S transect < 150 km east of the province-bounding fracture zone at 127°E ; we will refer to these as being

located in Zone A-west. Sites 1154, 1159, and 1160 were drilled further east in Zone A, and we shall refer to these as Zone A-east. *Christie et al.* [2001] provide full lithologic and petrographic details of the different sites. For ease of reference we briefly summarize each site in appendix A.

[10] The Leg 187 samples used for this study are predominantly holocrystalline basalts that are fresh to slightly altered (i.e., <10% secondary alteration). We analyzed glass-whole rock pairs in several cases in order to test for differing responses to alteration on isotopic composition. One totally altered basalt, one metabasalt, and a microgabbro from Site 1162 were also analyzed, as no fresh material was available from this site. In order to constrain the possible compositions of circulating fluids derived from overlying sediment, we analyzed a limestone sediment from Hole 1153, the dolomite breccia cement in Hole 1162B and palagonite separated from glass sample 1155B-8R-2, 5–9 cm. Brief petrographic descriptions of Leg 187 samples used in this study are provided in appendix A.

4. Provenance of Leg 187 Basalts

[11] The first objective of our study was to test whether Hf-Nd isotope systematics yield the same mantle provenance designation for individual samples as that produced by previously accepted criteria. As already mentioned, Pb isotopes have generally been regarded as the most robust geochemical criteria for distinguishing basalts of Indian versus Pacific mantle provenance. We therefore begin our analysis by evaluating the Pb isotope evidence for the provenance of Leg 187 basalts. Details of analytical procedures used at NIGL are provided in appendix B. Data are presented in Table 1.

4.1. Pb Isotope Evidence

[12] The global fields for Indian and Pacific MORBs are shown on a plot of $^{208}\text{Pb}/^{204}\text{Pb}$ versus $^{206}\text{Pb}/^{204}\text{Pb}$ in Figure 2. In this projection, Indian MORBs have generally higher $^{208}\text{Pb}/^{204}\text{Pb}$ for a given $^{206}\text{Pb}/^{204}\text{Pb}$. A linear discriminant boundary, identified statistically by discriminant analysis, is shown for reference. Figure 2 highlights the dis-

tinctive character of Indian MORB compared with Pacific MORB in Pb isotope space; less than 4% of the analyses lie outside of the relevant field boundaries or produce incorrect results in terms of provenance designation relative to the linear discriminant boundary (Figure 2b). Published data for recent on-axis basalts from the AAD are similarly distinguished, with most samples plotting in one of two groups: those with $^{206}\text{Pb}/^{204}\text{Pb}$ less than ~ 18.0 and those with $^{206}\text{Pb}/^{204}\text{Pb}$ greater than ~ 18.6 [*Klein et al.*, 1988; *Pyle et al.*, 1992]. Two samples from Zone B5 and one from Zone C have $^{206}\text{Pb}/^{204}\text{Pb}$ values that plot on the boundary between Indian and Pacific MORB. The samples from Zone B5 have been referred to as Transitional-Pacific by *Pyle et al.* [1995].

[13] Figure 3a presents the equivalent Pb isotope plot for Leg 187 samples, with published data for on-axis basalts shown as fields. Leg 187 lavas from Zones B4 and B5 plot entirely within the Indian MORB field. Basalts from Zone A-east plot as Pacific MORB and mostly within or near the field of on-axis Zone A basalts. Sites in Zone A-west are more complicated, and at least two of these include basalts derived from both mantle domains. All basalts from the two southern sites of the transect (Sites 1161 and 1162) are Indian MORB in character. Most of the basalts from Site 1158 are Pacific, but a sample from Hole 1158A is transitional in terms of $^{206}\text{Pb}/^{204}\text{Pb}$. Its higher $^{208}\text{Pb}/^{204}\text{Pb}$, however, suggests an Indian rather than Transitional-Pacific mantle provenance (Figure 3a). Basalts from Hole 1157B are also derived from Indian mantle, but both Indian and Pacific MORBs occur in Hole 1157A, showing the widest range of $^{206}\text{Pb}/^{204}\text{Pb}$ in any one hole (17.98–18.69; see Table 1). In contrast, all of the samples from Site 1153 are Transitional-Pacific in Pb-Pb isotope space, with $^{206}\text{Pb}/^{204}\text{Pb}$ values (18.31–18.43) intermediate between the two main groups; they overlap the compositions of Zone B5 lavas today. Thus, most of the linear array shown by the Leg 187 basalts is generated by lavas in Zone A, particularly Zone A-west. A logical interpretation of this observation is that the array is a function of mixing between an Indian mantle source like that feeding Zone B and a Pacific mantle source like that feeding Zone A.

Table 1. Sr, Nd-Pb-Hf Isotope Compositions of On-Axis and Leg 187 Basalts From the Australian-Antarctic Discordance

Hole	Sample no	rock type	zone	mantle domain	$^{87}\text{Sr}/^{86}\text{Sr}$	$^{143}\text{Nd}/^{143}\text{Nd}$	$\epsilon\text{Nd}(t_0)$	$^{176}\text{Hf}/^{177}\text{Hf}$	$\epsilon\text{Hf}(t_0)$	$^{206}\text{Pb}/^{204}\text{Pb}$	$^{207}\text{Pb}/^{204}\text{Pb}$	$^{208}\text{Pb}/^{204}\text{Pb}$	$^{206}\text{Pb}/^{204}\text{Pb}$ initial	$^{207}\text{Pb}/^{204}\text{Pb}$ initial	$^{208}\text{Pb}/^{204}\text{Pb}$ initial
Leg 187															
*1152A	1R-1, 25-29	bas	B4	IMM	0.703134	0.512978	6.59	0.283091	11.41	18.0625	15.4757	37.9914	18.027	15.476	37.966
1152B	4R-2, 20-24	bas	B4	IMM	0.703067	0.512987	6.77	0.283095	11.56	18.0625	15.4757	37.9871	18.042	15.476	37.970
*1163A	2R-2, 67-70	bas	B4	IMM	0.702996	0.513013	7.22	0.283107	11.88	18.0699	15.4704	37.9140	18.035	15.470	37.904
*1163A	3R-2, 2-6	bas	B4	IMM	0.703017	0.512999	7.01	0.283103	11.79	18.0494	15.4678	37.8998	18.031	15.468	37.887
1163A	6R-3, 46-49	bas	B4	IMM	0.703064	0.512992	6.83	0.283100	11.70	18.0767	15.4669	37.9281	18.054	15.467	37.912
*1163A	10R-1, 116-120	bas	B4	IMM	0.702995	0.512988	6.78	0.283105	11.86	18.0757	15.4633	37.9165	18.057	15.463	37.904
*1155A	2R-1, 29-32	bas	B5	IMM	0.702879	0.513031	7.62	0.283115	12.25	18.0937	15.4866	37.9063	18.083	15.487	37.897
*1155A	7R-1, 16-19	bas (L)	B5	IMM	0.702990	0.513026	7.52	0.283093	11.44	17.9871	15.4710	37.7631	17.966	15.471	37.750
*1155A	7R-1, 16-19	bas (UL)	B5	IMM	0.703346	0.513025	7.50	0.283088	11.25	17.996	15.481	37.806	17.975	15.481	37.792
1155B	4R-1, 76-80	bas	B5	IMM	0.702848	0.513049	7.95	0.283141	13.08	18.0056	15.4542	37.7568	17.974	15.454	37.742
1155B	6R-2, 140-144	bas	B5	IMM	0.702854	0.513055	8.04	0.283129	12.66	18.0061	15.4606	37.7819	17.993	15.461	37.771
1155B	8R-2, 5-9	bas	B5	IMM	0.702877	0.513039	7.74	0.283128	12.57	17.9982	15.4542	37.7597	17.968	15.454	37.733
1155B	8R-2, 5-9	gl	B5	IMM	0.702804	0.513048	7.92	0.283125	12.55	17.9968	15.4550	37.7611	17.975	15.455	37.746
1155B	8R-2, 5-9	gl (UL)	B5	IMM	0.702829	0.513042	7.80	0.283125	12.55	18.0078	15.4590	37.7713	17.986	15.459	37.756
1155B	8R-2, 5-9	pal	B5	IMM	0.704002	0.512944	8.19	0.283094	11.91	18.6859	15.6113	38.7683	18.675	15.611	38.766
1156A	2R-3, 18-24	bas	B5	IMM	0.702994	0.513010	7.19	0.283121	12.44	18.0288	15.4662	37.8457	17.998	15.466	37.833
*1156A	2R-3, 135-138	bas	B5	IMM	0.702921	0.513001	6.99	0.283103	11.79	18.0282	15.4649	37.8424	18.010	15.465	37.831
1156B	2R-1, 72-82	bas	B5	IMM	0.703017	0.513011	7.21	0.283097	11.58	18.0148	15.4642	37.8494	17.997	15.464	37.834
1156B	5R-1, 120-123	bas	B5	IMM	0.703007	0.512982	6.66	0.283105	11.87	18.0110	15.4642	37.8429	17.991	15.464	37.827
*1164A	4R-1, 20-24	bas	B5	IMM	0.702923	0.513033	7.64	0.283104	11.80	18.0418	15.4607	37.8584	18.007	15.461	37.845
1164A	4R-1, 20-24	bas	B5	IMM	0.702966	0.513015	7.29	0.283098	11.60	18.0444	15.4659	37.8719	18.026	15.466	37.863
1164B	3R-1, 93-97	bas	B5	IMM	0.702966	0.513005	7.08	0.283092	11.37	18.0469	15.4703	37.8838	18.036	15.470	37.875
1164B	10R-1, 21-25	bas	B5	IMM	0.702946	0.513001	6.99	0.283102	11.73	18.0664	15.4692	37.8911	18.042	15.469	37.884
1153A	7W-4, 5-8	ls	A-west		0.713078	0.512059	-11.38	0.282544	-8.18	18.7167	15.6297	38.9082	18.702	15.630	38.866
1153A	7W-4, 65-69	bas	A-west	TPMM	0.702758	0.513080	8.52	0.283156	13.66	18.3053	15.4716	37.9344	18.270	15.471	37.912
1153A	7W-4, 65-69	bas (UL)	A-west	TPMM	0.703248	0.513073	8.39	0.283156	13.66	18.3035	15.4722	37.9309	18.268	15.472	37.908
1153A	8R-1, 101-102	gl	A-west	TPMM	0.702734	0.513053	8.01	0.283138	13.06	18.4220	15.4864	38.0487	18.389	15.486	38.024
1153A	8R-1, 101-102	gl (UL)	A-west	TPMM	0.702777	0.513052	8.01	0.283138	13.06	18.4244	15.4849	38.0435	18.394	15.485	38.020
1153A	8R-1, 134-137	bas	A-west	TPMM	0.702942	0.513073	8.40	0.283129	12.75	18.4280	15.4884	38.0560	18.398	15.488	38.032
*1157A	1W-CC, 12-16	bas	A-west	IMM	0.702942	0.513021	7.39	0.283136	12.97	17.9848	15.4608	37.8079	17.970	15.461	37.796
*1157A	2R-1, 86-90	bas	A-west	PMM	0.702661	0.513066	8.26	0.283127	12.63	18.6920	15.5054	38.2420	18.669	15.505	38.227
1157A	3R-1, 30-32	bas	A-west	PMM	0.702729	0.513064	8.21	0.283128	12.68	18.6895	15.5027	38.2411	18.663	15.503	38.223
1157A	3R-1, 128-132	bas	A-west	PMM	0.702820	0.513061	8.17	0.283128	12.68	18.6493	15.4973	38.2084	18.620	15.497	38.190
1157B	3R-1, 55-58	bas	A-west	PMM	0.702867	0.513038	7.74	0.283167	14.08	17.9842	15.4560	37.7570	17.961	15.456	37.742
*1157B	6R-1, 43-47	bas	A-west	IMM	0.702913	0.513050	7.98	0.283162	13.90	17.9870	15.4566	37.7580	17.970	15.457	37.745
1157B	8R-1, 12-16	bas	A-west	IMM	0.702852	0.513060	8.18	0.283151	13.51	17.9854	15.4575	37.7611	17.963	15.457	37.743
*1158A	3R-1, 10-13	bas	A-west	IMM	0.703283	0.512982	6.66	0.283092	11.38	18.3142	15.4918	38.0910	18.283	15.492	38.076
1158B	4R-1, 111-114	bas	A-west	PMM	0.702725	0.513066	8.28	0.283123	12.50	18.5812	15.5001	38.1773	18.548	15.500	38.163

Table 1. (continued)

Hole	Sample no	rock type	zone	mantle domain	$^{87}\text{Sr}/^{86}\text{Sr}$	$^{143}\text{Nd}/^{143}\text{Nd}$	$\epsilon_{\text{Nd}(t)}$	$^{176}\text{Hf}/^{177}\text{Hf}$	$\epsilon_{\text{Hf}(t)}$	$^{206}\text{Pb}/^{204}\text{Pb}$	$^{207}\text{Pb}/^{204}\text{Pb}$	$^{208}\text{Pb}/^{204}\text{Pb}$	$^{206}\text{Pb}/^{204}\text{Pb}$ initial	$^{207}\text{Pb}/^{204}\text{Pb}$ initial	$^{208}\text{Pb}/^{204}\text{Pb}$ initial
1158C	2R-1, 45-50	diab	A-west	PMM	0.702676	0.513071	8.36	0.283133	12.85	18.6281	15.5020	38.1871	18.543	15.502	38.161
1161A	3R-1, 73-77	bas	A-west	IMM	0.702894	0.513080	8.55	0.283181	14.52	17.9743	15.4593	37.7460	17.959	15.459	37.735
1161A	4R-1, 120-124	bas	A-west	IMM	0.703028	0.513052	7.96	0.283173	14.25	17.9182	15.4557	37.6837	17.886	15.456	37.676
1161B	3R-1, 39-42	bas	A-west	IMM	0.702946	0.513033	7.64	0.283144	13.26	18.1564	15.4733	37.8952	18.134	15.473	37.880
1162A	5R-1, 25-30	mgab (L)	A-west	IMM	0.703579	0.513020	7.39	0.283154	13.43	18.2374	15.4797	37.7247	17.681	15.477	37.715
1162A	5R-1, 25-30	mgab (UL)	A-west	IMM	0.703679	0.513017	7.33	0.283154	13.43	18.3763	15.4908	37.7416	17.819	15.488	37.732
1162A	5R-2, 67-72	metabas	A-west	IMM	0.703080	0.513048	7.93	0.283173	14.26	18.0783	15.4757	37.7943	17.844	15.475	37.787
1162B	3R-2, 59-64	dolo	A-west	IMM	0.709057	0.512902	5.08	0.283133	12.85	17.2566	15.5057	37.055	17.125	15.505	37.018
1162B	6R-1, 69-74	alt bas (L)	A-west	IMM	0.703065	0.513073	8.42	0.283154	13.59	18.1385	15.4734	37.8509	17.582	15.471	37.841
1162B	6R-1, 69-74	alt bas (UL)	A-west	IMM	0.703501	0.513065	8.26	0.283154	13.59	18.1136	15.4755	37.8487	17.557	15.473	37.839
1154A	2R-1, 25-27	bas	A-east	PMM	0.702644	0.513100	8.91	0.283134	12.90	18.6170	15.4954	38.1483	18.556	15.495	38.125
1154A	9R-1, 46-50	bas	A-east	PMM	0.702629	0.513076	8.41	0.283137	13.01	18.5975	15.4878	38.1148	18.552	15.488	38.095
*1159A	2R-1, 20-24	bas	A-east	PMM	0.702627	0.513080	8.55	0.283124	12.50	18.7117	15.5054	38.2570	18.694	15.505	38.246
1159A	6R-2, 83-87	bas	A-east	PMM	0.702661	0.513072	8.39	0.283137	12.94	18.6604	15.5011	38.2166	18.651	15.501	38.209
1160A	3R-1, 19-21	bas	A-east	PMM	0.702542	0.513074	8.43	0.283113	12.11	18.8684	15.5203	38.3609	18.849	15.520	38.349
1160B	3R-1, 66-68	bas	A-east	PMM	0.702607	0.513076	8.40	0.283136	12.92	18.7161	15.4871	38.2132	18.705	15.487	38.207
*1160B	4R-2, 122-126	bas	A-east	PMM	0.702529	0.513107	8.99	0.283135	12.86	18.8201	15.5047	38.3221	18.809	15.505	38.314
*1160B	4R-2, 122-126	bas (UL)	A-east	PMM	0.702576	0.513096	8.73	0.283131	12.68	18.835	15.527	38.378	18.827	15.527	38.368
*1160B	9R-1, 127-129	bas	A-east	PMM	0.702576	0.513096	8.73	0.283131	12.68	18.7657	15.4981	38.2517	18.762	15.498	38.249
On-axis dredge samples															
D9-1		bas	C	IMM	0.702849	0.513017	7.35	0.283110	11.95	18.0908	15.4886	38.0125	18.0908	15.4886	38.0125
D10-10		bas	C	IMM	(0.70346)	0.513006	7.14	0.283163	13.83	17.7835	15.5084	37.8870	17.7835	15.5084	37.8870
D11-6		bas	C	IMM	(0.70283)	0.513040	7.80	0.283115	12.13	(17.944)	(15.409)	(37.743)	(17.944)	(15.409)	(37.743)
D8-6		bas	B1	IMM	0.703212	0.512988	6.79	0.283114	12.08	18.2441	15.4927	38.2809	18.2441	15.4927	38.2809
D7-3		gl	B3	IMM	(0.70290)	0.513007	7.16	0.283134	12.79	(18.057)	(15.439)	(37.858)	(18.057)	(15.439)	(37.858)
D7-3		bas	B3	IMM	(0.70290)	0.513012	7.26	0.283132	12.72	(18.057)	(15.439)	(37.858)	(18.057)	(15.439)	(37.858)
D7-7		gl	B3	IMM	(0.70300)	(0.51301)	7.22	0.283140	13.01	(18.008)	(15.462)	(37.794)	(18.008)	(15.462)	(37.794)
D7-7		bas	B3	IMM	(0.70300)	0.513035	7.71	0.283140	13.02	(18.008)	(15.462)	(37.794)	(18.008)	(15.462)	(37.794)
D5-5		bas	B5	PMM	(0.70255)	0.513074	8.47	0.283146	13.24	(18.572)	(15.482)	(38.097)	(18.572)	(15.482)	(38.097)
D1-2		gl	A3	PMM	(0.70264)	0.513065	8.29	0.283107	11.85	(18.805)	(15.499)	(38.262)	(18.805)	(15.499)	(38.262)
D1-2		bas	A3	PMM	(0.70264)	0.513072	8.43	0.283111	11.99	(18.805)	(15.499)	(38.262)	(18.805)	(15.499)	(38.262)
D2-19		bas	A3	PMM	(0.70261)	0.513072	8.43	0.283104	11.73	(18.911)	(15.514)	(38.319)	(18.911)	(15.514)	(38.319)
D3-4		bas	A3	PMM	(0.70257)	0.513058	8.15	0.283091	11.27	(18.979)	(15.590)	(38.416)	(18.979)	(15.590)	(38.416)
D4-1		bas	A3	PMM	(0.70253)	0.513086	8.70	0.283129	12.61	(18.816)	(15.504)	(38.155)	(18.816)	(15.504)	(38.155)
D6-1		bas	A2	PMM	(0.70259)	0.513077	8.52	0.283133	12.77	(18.617)	(15.480)	(38.095)	(18.617)	(15.480)	(38.095)

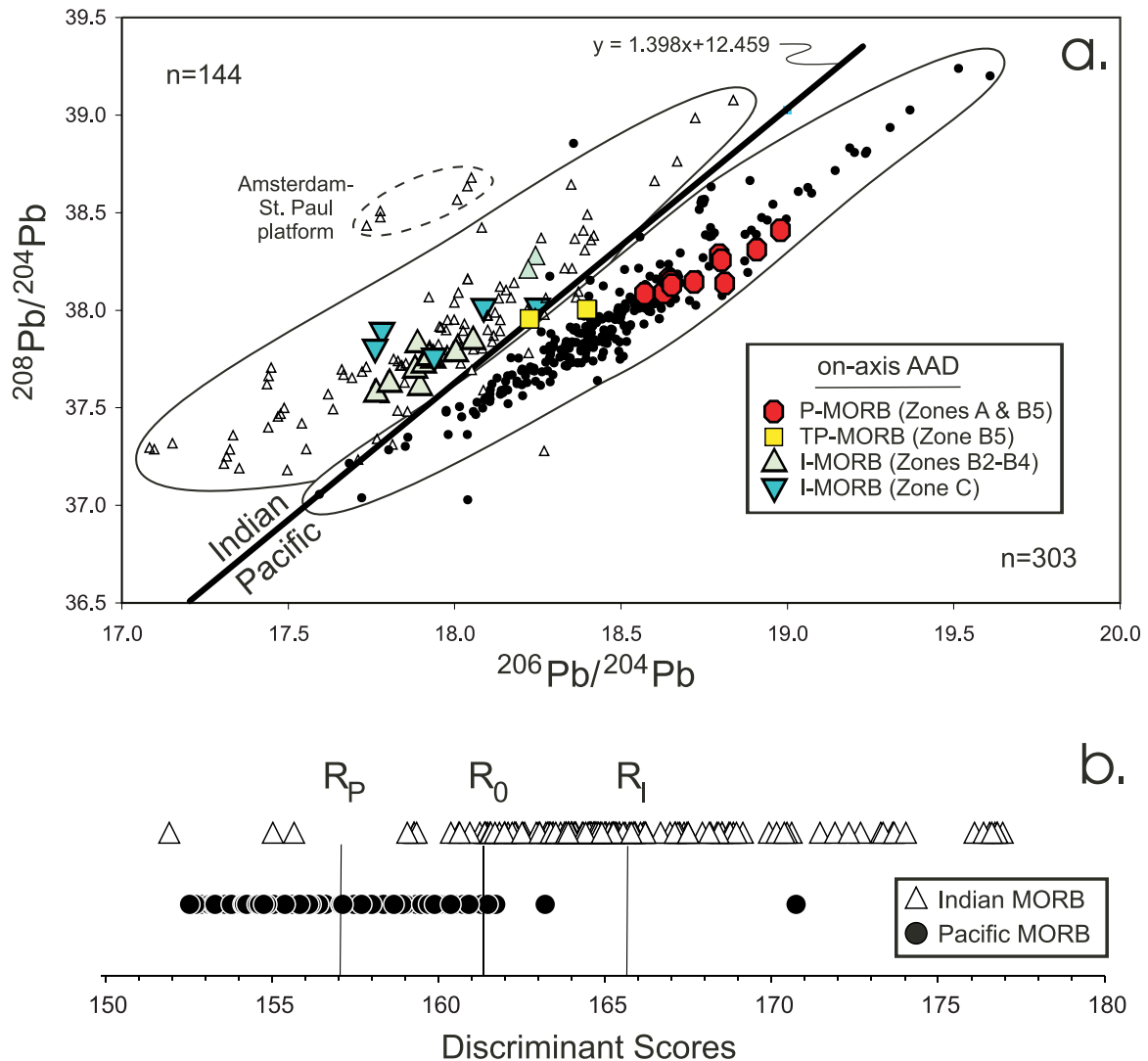


Figure 2. (a) Plot of $^{208}\text{Pb}/^{204}\text{Pb}$ versus $^{206}\text{Pb}/^{204}\text{Pb}$ for published data for on-axis basalts from the AAD [Klein *et al.*, 1988, 1991; Pyle *et al.*, 1992] compared with the global fields for Indian MORB (small open triangles) and Pacific MORB (small black dots). Data sources for MORB fields too numerous to mention, but available from the first author upon request. Note the Indian MORB field includes data from all three ridges within the Indian Ocean (SEIR, SWIR and CIR). The Pacific MORB field includes data for the Pacific-Antarctic Ridge as well as the East Pacific Rise. Equation for discriminant boundary shown is $^{208}\text{Pb}/^{204}\text{Pb} = (1.398 * ^{206}\text{Pb}/^{204}\text{Pb}) + 12.459$. In this and all subsequent diagrams I-MORB = Indian MORB, P-MORB = Pacific MORB, TP-MORB = Transitional-Pacific MORB. (b) Projection of Indian and Pacific MORB samples onto the discriminant function line, i.e., a line perpendicular to the boundary shown in (a). R_P is the projection of the bivariate mean of Pacific MORBs, R_I is the projection of the bivariate mean of Indian MORBs, and R_0 is the discriminant index, i.e., the point along the discriminant function line which is halfway between the centers of the two groups. Pacific samples that plot to the right of R_0 and Indian samples that plot to the left of R_0 are misclassified, i.e. 4% of the data shown. Equation for calculating the discriminant score is $R = (-18.109 * ^{206}\text{Pb}/^{204}\text{Pb}) + (12.950 * ^{208}\text{Pb}/^{204}\text{Pb})$. An F value of 418 (2 and 444 degrees of freedom) indicates that the discriminant function is significant at a >99% confidence level.

Notes to Table 1

^a Where leached and unleached pairs of samples occur, (L) denotes leached and (UL) unleached. All other data are as described in Appendix 2. Rock type abbreviations: bas = basalt whole rock; alt bas = altered basalt; metabas = metabasalt; mgab = microgabbro; gl = glass; diab = diabase; pal = palagonite; ls = limestone; dolo = dolomite. PMM = Pacific MORB-source mantle; TPMM = Transitional Pacific; IMM = Indian MORB-source mantle. Data in parentheses from Klein *et al.* [1988, 1991], all of which are basalt glass analyses except for D6-1, which is a whole rock. Rock type designations for on-axis samples refer to material analyzed at NIGL for Hf and Nd isotopes. Pb isotope analyses quoted to three significant digits were measured by TIMS; all others are PIMMS analyses. ϵHf and ϵNd values calculated assuming ages listed in Appendix 1. The asterisk indicates powders prepared for shipboard XRF; all other samples prepared according to procedures described in Appendix 2.

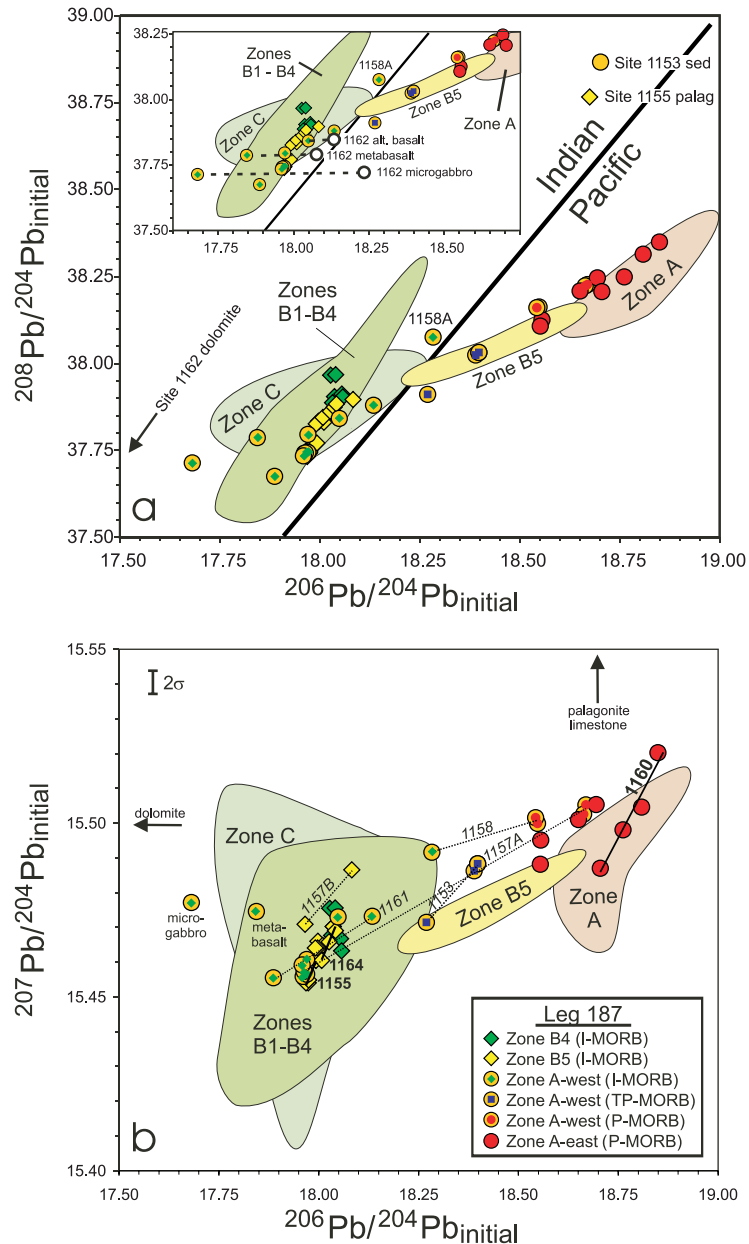


Figure 3. (a) Plot of $^{208}\text{Pb}/^{204}\text{Pb}_{\text{initial}}$ versus $^{206}\text{Pb}/^{204}\text{Pb}_{\text{initial}}$ for samples from Leg 187 compared with on-axis basalts from the AAD (shown as colored fields). Leg 187 data are from this study; on-axis data sources as in Figure 2. Discriminant boundary from Figure 2. Data shown have been age-corrected. For most samples, the correction is small [$<0.2\%$ on $^{206}\text{Pb}/^{204}\text{Pb}$ (see Table 1)], but for some highly altered (high U) samples from Site 1162, the effect is large (up to 3%). This is particularly true for the microgabbro, Sample 187-1162A-5R-1, 25-30 cm. Inset shows the difference between measured (open circles) and age-corrected data (filled circles), with data points for the same sample connected by a dashed line. Dolomite cement from Site 1162 plots outside the diagram to the left, whereas the limestone sediment (Site 1153) and palagonite (Site 1155) have radiogenic values of both $^{208}\text{Pb}/^{204}\text{Pb}$ and $^{206}\text{Pb}/^{204}\text{Pb}$ relative to Leg 187 basalts. Analytical uncertainty for PIMMS data (i.e., 2σ external reproducibility on standard measurements) is within the size of the symbols (see Appendix 2 for precise values). (b) Plot of $^{207}\text{Pb}/^{204}\text{Pb}_{\text{initial}}$ versus $^{206}\text{Pb}/^{204}\text{Pb}_{\text{initial}}$. Solid lines with steeper slopes connect data points from the same site or hole in Zones B4, B5 and A-east (site number indicated in bold text); dashed lines with shallower slopes connect data points from the same site or hole in Zone A-west (site number indicated in italics). Both palagonite and limestone have radiogenic $^{207}\text{Pb}/^{204}\text{Pb}$ values that plot outside the diagram; dolomite cement has a similar $^{207}\text{Pb}/^{204}\text{Pb}$ value to Leg 187 basalts but lower $^{206}\text{Pb}/^{204}\text{Pb}$, plotting outside the diagram to the left. As in Figure 3a the analytical uncertainty (2σ) for $^{206}\text{Pb}/^{204}\text{Pb}$ is less than the size of the symbol; the uncertainty on the $^{207}\text{Pb}/^{204}\text{Pb}$ measurement is shown as the solid black bar.

However, as will be shown below, this interpretation is only partially correct.

[14] The improved precision achieved by the plasma-ionisation multicollector mass spectrometry (PIMMS) analytical technique we have used (nearly one order of magnitude over TIMS, see appendix B), has enabled us to observe that, in at least a few cases, coherent trends exist within individual sites and/or holes. These trends differ in slope from the overall trend in Pb-Pb isotope space, particularly for $^{207}\text{Pb}/^{204}\text{Pb}$ versus $^{206}\text{Pb}/^{204}\text{Pb}$ (Figure 3b). They also differ in slope from one another, and therefore cannot share common end-members in most cases, even for sites from the same mantle domain. If the arrays are isochrons, those with steeper slopes (i.e., Sites 1155, 1160, and 1164; solid black lines on Figure 3b) imply ages of ~ 3 Ga, whereas those with shallow slopes (i.e., Sites 1153, 1158, 1157, and 1161; dotted lines on Figure 3b) imply ages of ~ 1 Ga. We do not wish to overinterpret the age significance of these data, as the number of analyses per site is small in most cases and our data are predominantly for whole rock samples rather than hand-picked basaltic glasses (hence potential complications from the effects of alteration and age correction). It is also possible that the arrays represent mixing, particularly those with shallower slopes (note that the shallower slopes are all from sites in Zone A-west). Regardless, the observation is consistent with similar findings for Pacific MORBs [Galer *et al.*, 2000] and, at the very least, calls into question the notion of a shallow, depleted mantle that is convectively well-mixed and relatively homogeneous.

4.2. Nd-Hf Isotope Evidence

4.2.1. Provenance of On-Axis Basalts

[15] On the basis of Hf isotope data for MORB reported by *Salters* [1996], *Pearce et al.* [1999] recognized that the field of Indian MORB is offset from that of Pacific MORB in Nd versus Hf isotope space. They also showed that this difference could be a valuable tool for the study of mantle provenance, applying it in particular to the arc-back arc basin settings of the western Pacific. However, the Hf isotope database for MORB is relatively small and, until recently [Kempton *et al.*,

2000; *Chauvel and Blichert-Toft*, 2002], was collected using older and generally less precise analytical techniques than are now available. As the distinctions we are trying to make in this study are small in some cases, it has been necessary to exclude most of the older analyses from our investigation. The 43 new PIMMS Hf isotope analyses for Atlantic, Pacific, and Indian MORBs reported by *Chauvel and Blichert-Toft* [2002] significantly increase the size of the available database; although given the $>60,000$ km of mid-ocean ridges that encircle the globe, they encompass only a limited geographic range. For example, most of the data for Indian MORBs by *Chauvel and Blichert-Toft* [2002] come from near the Rodrigues Triple Junction (within ~ 1000 km), which is almost 4000 km away from the AAD.

[16] Therefore, for comparative purposes, we have determined the Hf and Nd isotope compositions of recent, on-axis samples from the AAD, together with the older, off-axis basalts from Leg 187. Our new data for the on-axis samples are presented in Table 1 and shown in Figure 4a relative to fields for Indian and Pacific MORB based on published data. Figure 4 also shows our statistically determined discriminant boundary, revised from *Pearce et al.* [1999] to take into account the new data reported here and by *Chauvel and Blichert-Toft* [2002].

[17] On-axis basalts from Zone A extend the previous field for Pacific MORB to lower values of both ϵNd and ϵHf (Figure 4a). Compared with the global database, they encompass only a small range of compositions ($\epsilon\text{Nd} = +8.2$ to $+8.7$). All plot well below the mantle array correlation line defined by *Vervoort et al.* [1999], as do most basalts derived from Pacific mantle. Note that all of the published Hf isotope data for Pacific MORBs come from locations north of 21°N , i.e., from the northern Pacific domain as defined by *Vlastelic et al.* [1999]. According to these authors, Pacific MORBs from the southern domain (i.e., the EPR south of 21°N and the Pacific-Antarctic Ridge) are characterized by lower ϵNd and higher $^{206}\text{Pb}/^{204}\text{Pb}$ ratios than MORBs from the northern domain. The new data for on-axis basalts from east of the AAD are consistent with this compositional distinction

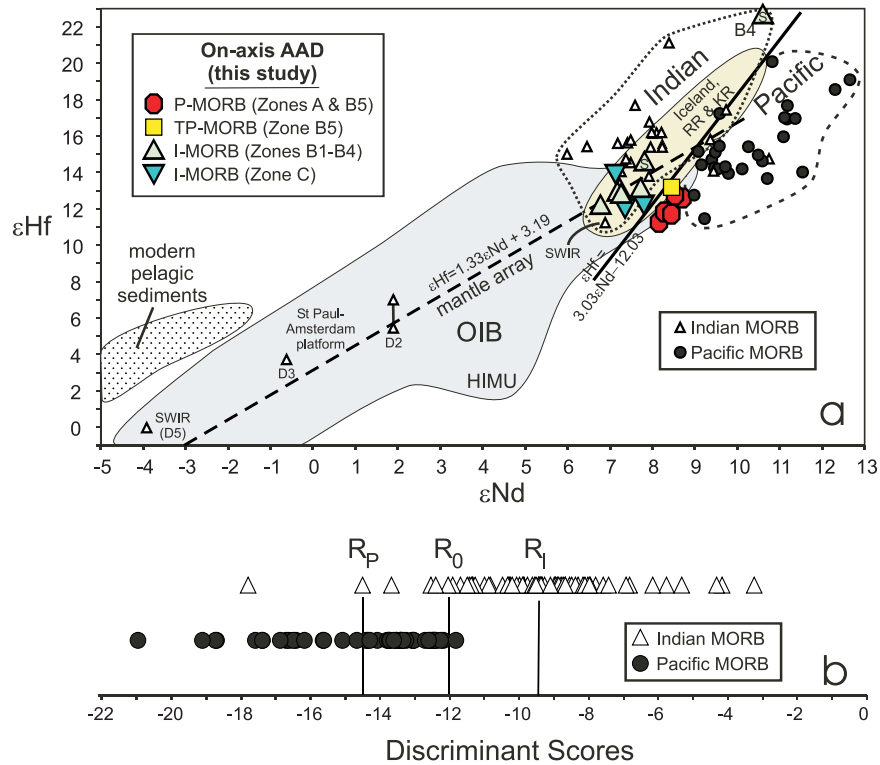


Figure 4. (a) Plot of ϵHf versus ϵNd comparing on-axis AAD samples with global fields for OIB, Pacific MORB and Indian MORB. AAD data are from this study, plus two Hf analyses from *Salters* [1996]; Nd analyses for the latter are from *Pyle et al.* [1992] and P. D. Kempton (unpublished data, 2001). The *Salters* [1996] data are shown as green triangles labeled with the letter S; an unusually depleted basalt from Zone B4 is further distinguished by the label B4. Other Indian and Pacific MORB data from *Patchett* [1983], *Salters* [1996], *Nowell et al.* [1998], *Salters and White* [1998], *Chauvel and Blichert-Toft* [2002] and P. D. Kempton (unpublished data, 2001). Note that we have filtered the literature data to exclude analyses having a within-run standard error greater than 100 ppm. Even this cut-off is approximately five times our own typical within-run precision and twice our external analytical uncertainty, based on replicate standard analyses. The error on the unusually depleted rock from Zone B4 [*Salters*, 1996] slightly exceeds this criteria, but has been included because it is the only published analysis for this highly radiogenic sample. The unusual composition of samples from this zone has been confirmed by *Hanan et al.* [2000] and within our own laboratory (P. D. Kempton, unpublished data). We have also excluded older published data for samples that have been reanalyzed by *Chauvel and Blichert-Toft* [2002] or during the course of this study (see Table 1). Duplicate analyses of SEIR sample MD37-18-06-D2 from *Chauvel and Blichert-Toft* [2002] are joined by solid black tie line. OIB field modified from *Nowell et al.* [1998]. Pelagic sediment data are from *Vervoort et al.* [1999]. Our proposed discriminant boundary is shown as the solid black line ($\epsilon\text{Hf} = 3.031 \cdot \epsilon\text{Nd} - 12.033$ or $^{176}\text{Hf}/^{177}\text{Hf} = 1.7138 \cdot ^{143}\text{Nd}/^{144}\text{Nd} - 0.59615$); the Indian MORB data set used to calculate the discriminant boundary excludes the three plume-related samples with unusually low Nd isotope ratios. The terrestrial array (or crust-mantle correlation line) from *Vervoort et al.* [1999] is shown as a dashed line. (b) Projection of Indian and Pacific MORB samples onto the discriminant function line. See Figure 2 for definition of R_p , R_1 and R_0 . Equation for calculating the discriminant score is $R = (-3.0226 \cdot \epsilon\text{Nd}) + (0.9971 \cdot \epsilon\text{Hf})$. An F value of 71.805 (2 and 116 degrees of freedom) indicates that the discriminant function is significant at a >99% confidence level; only 6% of the data is misclassified by the discriminant boundary shown in Figure 4a.

and suggest that the southern Pacific domain has lower ϵHf as well as lower ϵNd .

[18] On-axis samples from Zones B and C are compositionally more diverse than those from Zone A, particularly in terms of their Nd isotope

ratios; they are offset to lower ϵNd , with ϵHf values that are similar to or higher than those of Zone A basalts. With the exception of the unusually depleted rocks from Zone B4 [*Salters*, 1996; *Hanan et al.*, 2000], the on-axis basalts from Zones B and C have Hf isotope ratios that are lower than

those from most other locations in the Indian Ocean; they plot on or below the mantle array correlation line rather than above it. In this regard, the Indian MORB field is not unlike the field of plume-related magmatism on the Reykjanes and Kolbeinsey ridges adjacent to Iceland (Figure 4a) [Kempton *et al.*, 2000]. Two SEIR samples analyzed by Chauvel and Blichert-Toft [2002] have particularly enriched compositions (MD37-18/06-D2 and MD37-18/06-D3); but this is consistent with a strong plume signature based on other geochemical characteristics of these samples, as well as their geographic location on the southern flank of the St. Paul-Amsterdam platform rather than on the ridge axis as strictly defined [Dosso *et al.*, 1988]. Similarly, sample MD34-D5 from the SWIR is renowned for its unusually unradiogenic Pb and Nd isotope ratios and ambiguous origin [Mahoney *et al.*, 1996].

[19] Most important for our purposes is the fact that Indian and Pacific MORBs are clearly distinguishable in Nd-Hf isotope space. One basalt from the Central Indian Ridge (Hf isotopes from Chauvel and Blichert-Toft [2002]; Nd isotopes from Michard *et al.*, [1986]) plots well within the Pacific MORB field, as do two gabbros from Hole 735B on the Southwest Indian Ridge [Nowell *et al.*, 1998]. Whether this is due to analytical uncertainty or the presence of a Pacific/Atlantic-type component beneath these ridges that may not be present beneath the SEIR west of the AAD is unknown. Clearly the level of analytical uncertainty associated with both Nd and Hf isotope data (i.e., $\sim 25\text{--}50$ ppm, 2σ) means that an individual sample plotting within <0.5 epsilon unit of the boundary cannot be unambiguously assigned a mantle provenance unless other supporting data are available. Nonetheless, $\sim 95\%$ of the available data are properly discriminated by this diagram, which is only marginally less successful than the $^{208}\text{Pb}/^{204}\text{Pb}$ versus $^{206}\text{Pb}/^{204}\text{Pb}$ diagram (compare Figures 2b and 4b).

4.2.2. Provenance of Leg 187 Basalts

[20] Leg 187 basalts overlap the range of ϵHf and ϵNd values exhibited by the on-axis samples (Table 1 and Figure 5). However, many of the Indian

MORBs from Leg 187 have ϵHf values that are less radiogenic than those of on-axis basalts from either Zone B or Zone C today ($\epsilon\text{Hf} < +12$). Note that because we have no a priori geographical evidence for the mantle provenance of the Leg 187 samples, this have been assigned on the basis of the Pb isotope discriminant (Figure 3a). The fact that there is almost no overlap between Indian and Pacific MORBs in Figure 5 indicates that the $\epsilon\text{Hf} - \epsilon\text{Nd}$ discriminant yields the same result in terms of mantle provenance as Pb isotopes, even for the older off-axis basalts.

[21] The samples from Site 1153 that have transitional $^{206}\text{Pb}/^{204}\text{Pb}$ are similarly transitional in ϵHf versus ϵNd , with one sample plotting above, one below and one on the discriminant boundary (Figure 5). In contrast, the sample from Hole 1158A that has transitional $^{206}\text{Pb}/^{204}\text{Pb}$ is clearly derived from Indian mantle based on its $\epsilon\text{Hf} - \epsilon\text{Nd}$ isotopic signature.

[22] An interesting feature of the data from Leg 187 is that Hf isotope composition appears to correlate with geographic location; basalts derived from Indian mantle in Zone A-west tend to have more radiogenic Hf and Nd isotope compositions than Indian MORBs from Zone B (i.e., indicating greater time-integrated depletion of the source; Figure 5). They also have higher ϵHf values than Pacific MORBs from Zone A-east. This contrasts with the Pb isotope results, where the lavas collectively appear to represent mixtures of just two end-members: Zone B-like Indian mantle and Zone A-like Pacific mantle.

[23] This distinction is emphasised in a plot of ϵHf versus initial $^{206}\text{Pb}/^{204}\text{Pb}$ ratios (Figure 6). Leg 187 basalts derived from Indian mantle show a wide range of ϵHf values for only a very small range in $^{206}\text{Pb}/^{204}\text{Pb}$: those from Zones B4 and B5 occupy the less depleted (lower ϵHf) end of the array and those from Zone A-west the more depleted (higher ϵHf) end. The most depleted Pacific MORB compositions have lower ϵHf and higher $^{206}\text{Pb}/^{204}\text{Pb}$ values that are unlike the depleted Indian MORB basalts from Zone A-west. However, the older off-axis basalts from Zone A are skewed toward lower $^{206}\text{Pb}/^{204}\text{Pb}$ values than on-axis basalts. Collec-

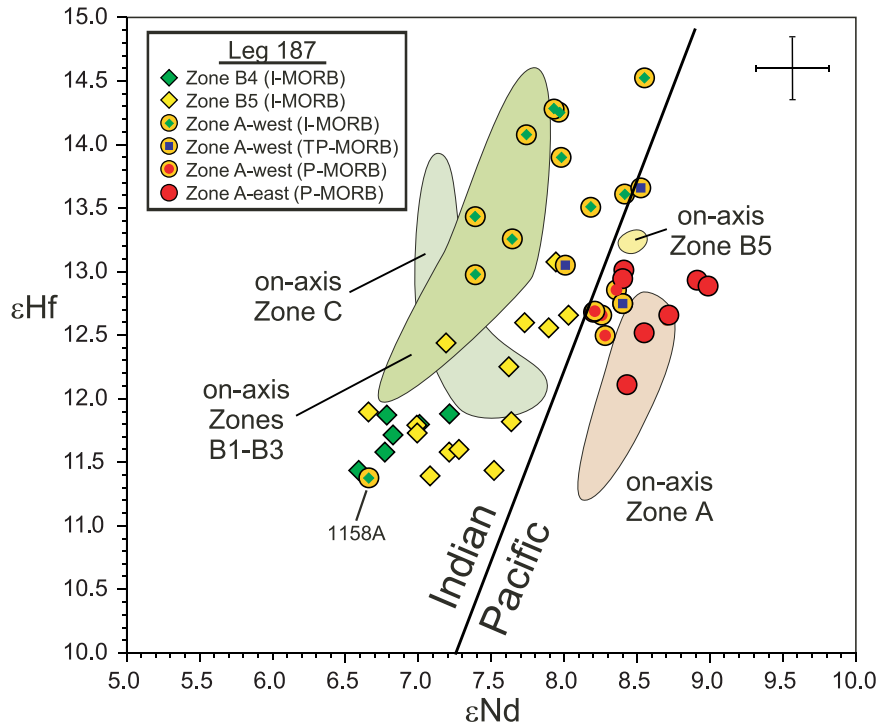


Figure 5. Plot of ϵHf versus ϵNd comparing Leg 187 basalts (this study) with the compositions of on-axis samples from Figure 4a shown as fields. Discriminant boundary from Figure 4a.

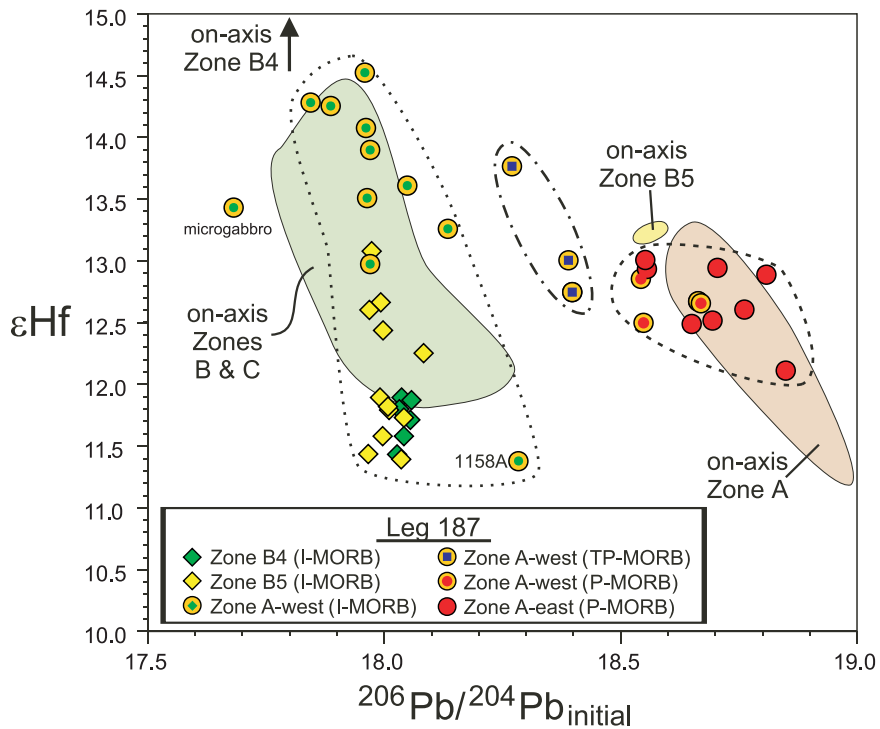


Figure 6. Plot of ϵHf versus $^{206}\text{Pb}/^{204}\text{Pb}_{(\text{initial})}$. Data sources for on-axis samples as in Figure 3.

tively, they generate a broad array with a negative slope that trends toward the depleted end of the Indian MORB array and passes through the compositions of Transitional-Pacific basalts from Site 1153. This suggests that the rocks from Site 1153, and possibly some Pacific MORB basalts from Zone A, are indeed mixtures between Indian and Pacific MORB (i.e., their source region encompasses the isotopic mantle domain boundary), but the depleted end-member is specifically the depleted Indian MORB mantle found beneath parts of Zone A-west.

5. Major and Trace Element Data

[24] Major and trace element data for Leg 187 basalts included in this study are provided in Table 2. Analytical details can be found in appendix B. Shipboard comparisons of whole rock and glass samples showed that MgO contents are consistently lower in analyses of whole rock powders relative to associated glass separates [Christie *et al.*, 2001]. This is believed to be due to release of MgO during replacement of both phenocryst and groundmass olivine by Fe-oxyhydroxides. In contrast, other major elements and most trace elements appear to be unaffected in most cases. Therefore, although we present the major element data for our samples for completeness, we have not used these data for petrogenetic modeling because their Mg # would not adequately reflect the composition of the original magma. Instead, we focus on trace element (and isotopic) characteristics.

5.1. Comparison of Indian and Pacific MORBs From Leg 187

[25] Although absolute abundances vary, the trace element patterns of most Leg 187 basalts have similar shapes on primitive-mantle-normalised plots, regardless of mantle provenance (Figure 7). All are light rare earth element (LREE) depleted, and most lie within the range of published data for on-axis basalts (Figures 7a–7b), the most notable exception being some highly depleted basalts from Hole 1160B. This hole was drilled on the flank of a seamount, and the basalts from this location are inferred to have formed from higher degrees of melting [Christie *et al.*, 2001], which is consistent

with their lower large-ion lithophile element (LILE), La/Yb and heavy rare earth element (HREE) abundances. Indian MORBs from Leg 187 encompass a slightly greater range in trace element abundances than Indian MORBs from on-axis, but Leg 187 basalts from Zones B and A-west show similar ranges in composition to one another (Figure 7a). Other differences among the various groups are more subtle and easiest to see using average values (Figure 7c) or plots of trace element ratios (Figure 8).

[26] Excluding the depleted rocks from Hole 1160B, the average Pacific MORB composition for Leg 187 has higher HREE abundances than the Indian MORB averages for Zones B and A-west (Figure 7c). The degree of enrichment decreases for elements to the left of Nd, and concentrations overlap at La, resulting in a slightly more depleted (lower La/Yb) trace element signature for average Pacific MORB. Conversely, Indian MORBs from Zone B have the least depleted trace element patterns. The average Transitional-Pacific basalt is similar to average Pacific MORB in its ratio of LREE to HREE, but it has trace element abundances indistinguishable from Indian MORBs from Zone B for elements to the right of Nd.

[27] These differences are emphasised in Figure 8a, a plot of La/Yb versus $^{87}\text{Sr}/^{86}\text{Sr}$. In this figure Leg 187 samples form a broad positive array in which Zone B4 Indian MORBs have the highest ratios and Pacific MORBs the lowest ratios. Indian MORBs from Zones B5 and A-west are intermediate between these two end-members, with some of the more altered samples scattering to higher $^{87}\text{Sr}/^{86}\text{Sr}$. Sr isotope composition also correlates negatively with Zr/Nb (Figure 8c). Conversely, Zr/Nb, Nb/Y, and La/Nb (not shown) correlate positively with ϵHf and ϵNd (Figures 8b and 8d). Because these trace element ratios correlate with isotopic composition, at least some of the variation must be due to differences in source composition and not magmatic processes (i.e., degree of partial melting and/or fractional crystallization). Furthermore, as with isotope-isotope covariations (e.g., Figure 6), it is clear that two component mixing cannot explain the data, since the order of the

Table 2. Major and Trace Element Analyses of Leg 187 Basalts [The full Table 2 is available in the HTML version of the article at <http://www.g-cubed.org>.]

Hole	*1152A	1152B	1152B	*1163A	1163A	1163A	1163A	1163A	1163A	*1163A	1163A	1163A	*1155A	1155A	1155B
Core	1R-1	4R-2	6R-1	2R-2	3R-1	4R-1	6R-3	9R-1	9R-1	10R-1	10R-1	10R-1	2R-1	7R-1	4R-1
cm.	25–29	20–24	43–49	67–70	22–28	11–14	46–49	93–97	93–97	116–120	120–122	29–32	16–19	76–80	
Zone	B4	B4	B4	B4	B4	B4	B4	B4	B4	B4	B4	B5	B5	B5	B5
Type	AB	PB	PB	PB	PB	AB	AB	AB	AB	AB	AB	PB	AB	AB	PB
SiO ₂	50.38	51.44	50.46	49.34	49.80	49.37	49.94	50.15	49.72	49.93	50.11	48.33	49.12	49.21	49.21
Al ₂ O ₃	14.69	15.14	15.75	15.93	16.68	15.59	15.96	15.74	15.58	15.38	15.76	16.06	16.48	17.38	17.38
Fe ₂ O ₃	11.03	9.18	9.19	7.77	8.47	9.22	9.45	9.63	9.39	9.39	9.60	9.08	9.28	8.54	8.54
MgO	5.80	7.40	6.28	8.24	8.67	7.87	8.32	8.11	8.15	7.91	8.06	6.88	7.23	8.10	8.10
CaO	10.67	11.72	12.17	12.76	12.27	11.29	11.23	11.27	11.36	11.24	11.22	11.58	11.80	11.80	11.80
Na ₂ O	3.07	2.80	2.88	2.56	2.48	2.83	2.75	2.70	2.75	2.79	2.70	2.83	2.68	2.55	2.55
K ₂ O	0.433	0.261	0.381	0.170	0.133	0.240	0.248	0.249	0.276	0.26	0.246	0.300	0.23	0.195	0.195
TiO ₂	2.050	1.608	1.625	0.930	0.979	1.310	1.367	1.420	1.385	1.35	1.406	1.660	1.16	1.009	1.009
MnO	0.162	0.172	0.161	0.120	0.144	0.140	0.154	0.159	0.153	0.14	0.157	0.150	0.14	0.138	0.138
P ₂ O ₅	0.227	0.156	0.157	0.080	0.079	0.170	0.158	0.160	0.160	0.17	0.158	0.200	0.12	0.090	0.090
LOI	0.95	-0.19	0.54	0.64	0.08	1.24	0.19	0.11	0.52	0.79	0.32	1.18	1.64	0.60	0.60
Total	99.46	99.65	99.48	98.54	99.79	99.27	99.76	99.69	99.44	99.35	99.73	98.25	99.88	99.61	99.61
Sc	39.2	40.8	38.0	32.6	30.7	33.3	33.5	35.1	32.0	34.5	34.7	32.3	34.7	30.5	30.5
V	339	302	297	213	198	249	248	249	241	258	253	264	238	194	194
Cr	242	358	287	442	412	383	367	350	344	375	351	320	416	345	345
Co	42.3	38.1	36.4	44.9	38.0	40.9	37.0	37.0	37.5	40.8	40.8	40.8	40.9	40.9	40.9
Ni	130	95	63	139	158	154	183	162	188	138	168	128	123	172	172
Cu	53	58	60	63	59	56	51	47	50	54	50	52	63	60	60
Zn	102	86	80	72	63	80	77	78	76	79	79	81	73	64	64
Ga	18.1	16.3	17.5	14.5	14.1	16.2	16.1	15.4	14.6	16.7	16.8	16.5	15.8	14.8	14.8
Rb	6.85	2.85	3.40	2.60	1.73	1.92	1.96	1.42	2.56	2.04	1.64	3.81	3.62	3.39	3.39
Sr	135	141	139	130	109	172	166	156	149	159	160	133	160	123	123
Y	44.1	34.7	35.5	21.9	21.6	30.1	29.7	30.6	28.6	31.5	31.6	36.6	25.3	23.4	23.4
Zr	157.4	114.4	118.3	120.4	57.3	109.7	107.8	107.8	101.5	110.4	110.9	134.1	83.3	65.9	65.9
Nb	4.22	2.75	2.95	0.98	0.98	3.25	3.20	3.01	2.78	2.92	3.09	3.67	2.49	1.48	1.48
Cs	0.46	0.05	0.07	0.13	0.03	0.03	0.04	0.02	0.08	0.05	0.02	0.10	0.28	0.22	0.22
Ba	23.6	24.6	7.3	4.7	4.3	13.3	12.1	11.2	9.4	11.2	11.5	9.6	9.9	9.9	9.9

AB = aphyric basalt; PB = phyrific basalt; GL = glass; DIAB = diabase; PAL = palagonite; DOLO = dolomite cement; MB = metabasalt; MG = microgabbro; APB = altered phyrific basalt. In the main Table, XRF analyses for Sc, V, Cr, Ni, Cu, Zn, and Rb through Nb are reported for most samples; where XRF data are unavailable, Sc, V, Cr, Ni, Cu and Zn values from ICP-MS are reported; samples to which this applies are listed at the end of the table caption. XRF trace element data indicated using bold text. Elements Co, Ga and Rb through U were determined by ICP-MS. Appendix 2 gives the methods of analysis and discusses interlaboratory comparisons. The ICP-MS analyses of three international standard samples and one laboratory standard (X108) not forming part of the calibration are listed together with σ RSD values for multiple within-analysis variations of W2 (RSD1; n = 20) and for separate preparations of JBI (RSD2; n = 3). Details of X108 are given in *Peate et al.* [2001]. Samples were ground in agate except those prepared for shipboard analysis (identified with an asterisk), which were ground in tungsten carbide. Most of the latter can be identified by the fact that Ta and Co are not quoted because of excessive contamination, and Nb is given in italics because an empirical contamination correction had to be made to the measured value (typically 0.4 ± 0.2 ppm depending on the quantity of added W and Ta). Samples for which a correction has been applied to the Nb ICP-MS value include: 1163A-3R-2, 67–70 cm, 1163A-10R-1, 116–120 cm, 1155A-2R-1, 29–32 cm, 1155A-7R-1, 16–19 cm, 1155B-9R-2, 63–67 cm, 1164A-4R-1, 20–24 cm, 1157A-2R-1, 86–90 cm, 1157B-6R-1, 43–47 cm, 1158A-3R-1, 10–13 cm, 1160A-3R-1, 19–21 cm. Samples for which ICP-MS values for Sc, V, Cr, Ni, Cu and Zn are reported include: 1163A-2R-2, 67–70 cm, 1163A-3R-2, 2–6 cm, 1163A-10R-1, 116–120 cm, 1155A-2R-1, 29–32 cm, 1155A-7R-1, 16–19 cm, 1155B-8R-2, 5–9 cm, 1155B-9R-2, 63–67 cm, 1164A-4R-1, 20–24 cm, 1153A-7W-4, 5–8 cm, 1157A-2R-1, 86–90 cm, 1157B-6R-1, 43–47 cm, 1158A-3R-1, 10–13 cm, 1162B-3R-2, 59–64 cm, 1159A-2R-1, 20–24 cm, 1160A-3R-1, 19–21 cm, 1160B-4R-2, 122–126 cm.

groups along each trend is different from one diagram to another. For example, compare Figures 8a and 8c, where Zone A-west basalts are compositionally intermediate between Zone A-east and Zone B, with Figure 8d, where Zone A-west appears to be the depleted end-member.

5.2. Effects of Alteration

[28] Alteration has clearly affected many of the LIL elements, even in the visibly freshest rocks. Cs and Rb are strongly enriched in all samples (Fig-

ures 7a–7b). Pb and U concentrations are variable but generally enriched relative to adjacent elements on plots of normalised trace element composition. The limestone sediment and dolomite cement (Figure 9a) also show extreme enrichments in Pb and U, as well as the LREE and LILE, but relatively low concentrations of the HREE and high field strength element (HFSE).

[29] In contrast to the mobility of Pb and U, REE and HFSE contents of the basalts appear to be largely unaffected by alteration, even where this is extensive. Sample 1162B-6R-1, 69–74 cm is totally altered to clays + Fe-oxyhydroxides (see appendix A), yet for most elements it has a trace element pattern indistinguishable from the rest of the basalts from Leg 187 (Figure 9a), the most notable exception being its strong enrichment in U.

[30] The palagonite separated from sample 1155B-8R-2, 5–9 cm has very low concentrations of all the REE except Ce, combined with strong enrichments in HFSE as well as Pb, U, Cs, Rb, and Sr (Figure 9b). The palagonite also has high $^{206}\text{Pb}/^{204}\text{Pb}$, $^{207}\text{Pb}/^{204}\text{Pb}$, and $^{208}\text{Pb}/^{204}\text{Pb}$ relative to the AAD basalts (Figure 3; Table 1) but has a similar Pb

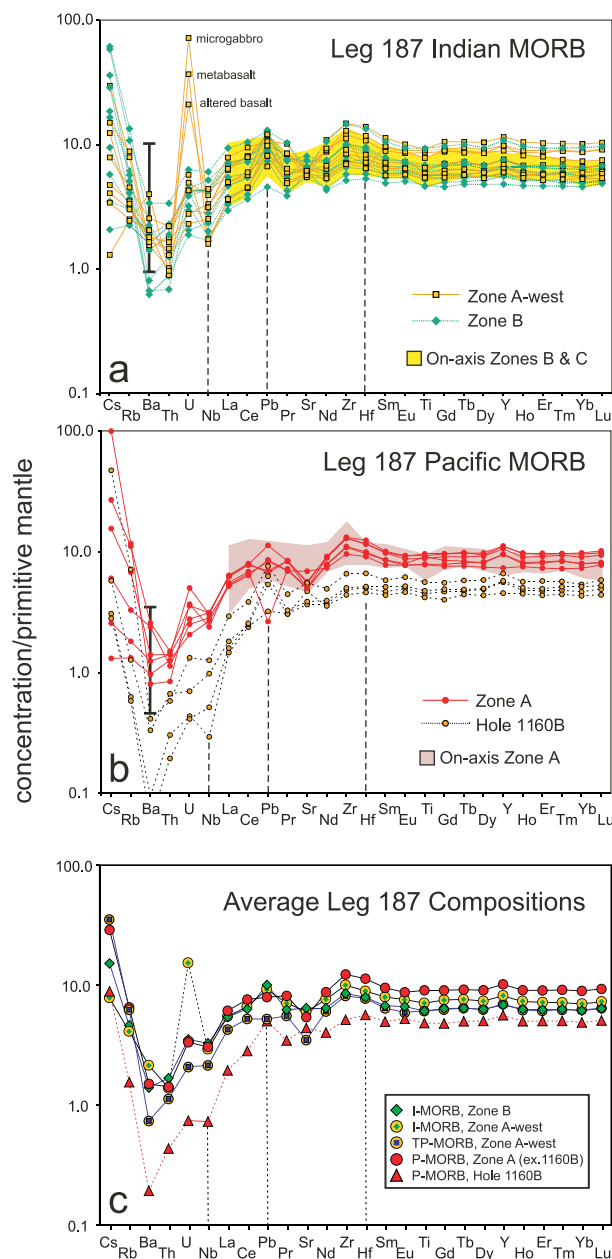


Figure 7. (opposite) Extended trace element plots for basalts from Leg 187. (a) Representative samples of Indian MORBs from Zones B and A-west, selected to encompass the range of compositions observed in each zone. Yellow field shows the range of published data for on-axis Indian MORBs from Zones B and C; data from Klein *et al.* [1988] and Pyle *et al.* [1995]. Cs, Rb, Th, U and Nb have been excluded from the field of literature data because only 3 analyses have been published that include these elements [Pyle *et al.*, 1995], which is insufficient to establish a representative range; the range for Ba is shown as the vertical black line. The three Leg 187 samples with high U concentrations are highly altered rocks from Site 1162. (b) Representative samples of Pacific MORBs from Zone A. Basalts from Hole 1160B are shown separately because of their unusually depleted compositions relative to other Zone A basalts. The red field shows the range of on-axis Pacific MORBs from Zone A; data from Klein *et al.* [1988] and Pyle *et al.* [1995]. (c) Average compositions for basalts shown in figures a and b. Note that if we exclude the highly altered rocks from Site 1162, the U concentration for Indian MORBs from Zone A-west is indistinguishable from the other average compositions; the average value if these samples are included is indicated by the dashed lines. Normalising values of Sun and McDonough [1989].

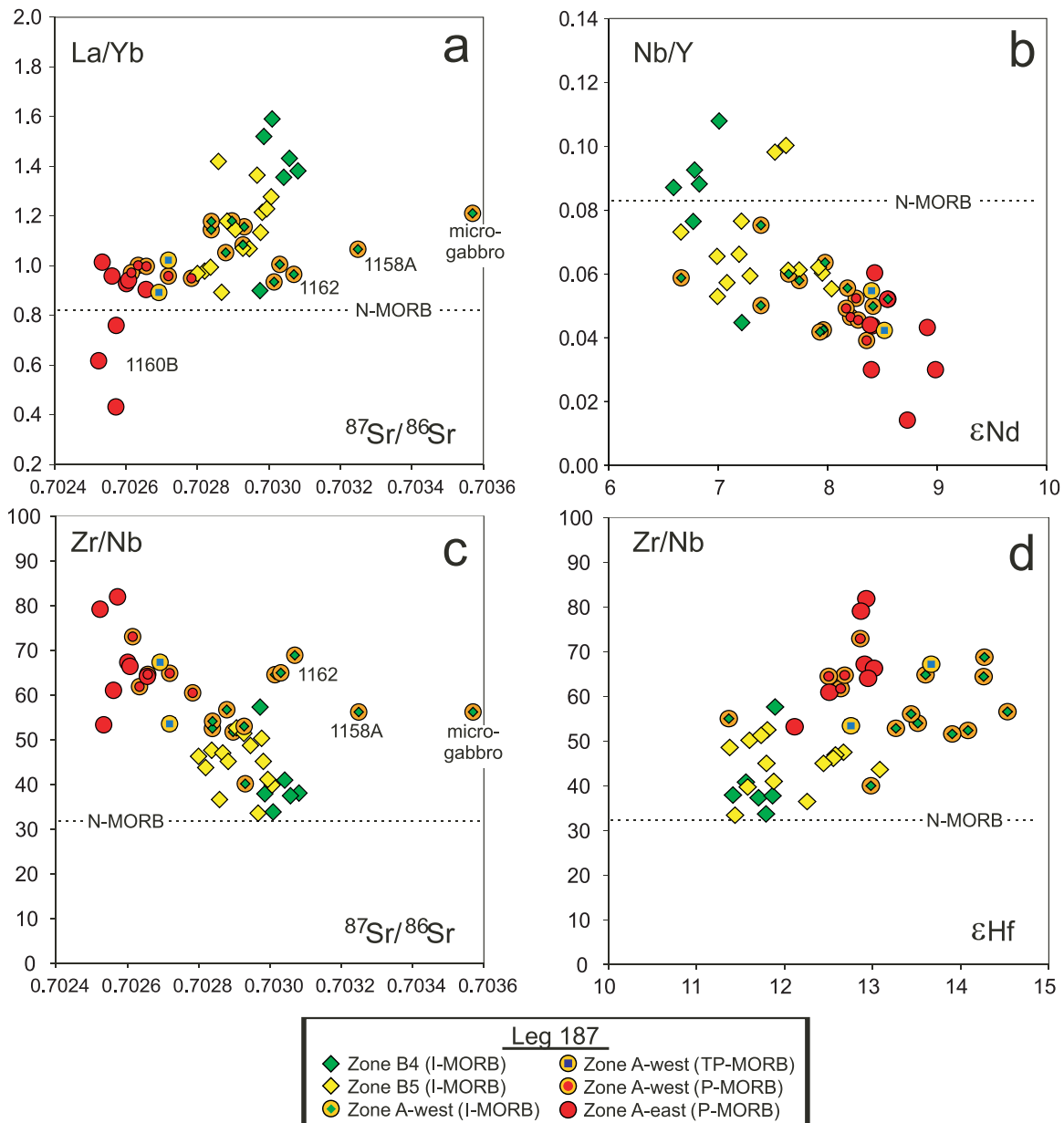


Figure 8. Isotopes versus trace element ratio plots for Leg 187 basalts. (a) La/Yb versus $^{87}\text{Sr}/^{86}\text{Sr}$. (b) Nb/Y versus ϵNd . (c) Zr/Nb versus $^{87}\text{Sr}/^{86}\text{Sr}$. (d) Zr/Nb versus ϵHf . Average N-MORB for Zr/Nb, La/Yb and Nb/Y [Sun and McDonough, 1989] are indicated by dotted horizontal lines. Zr contents determined by ICP-MS and XRF differ outside of analytical uncertainty for the microgabbro, Sample 1162A-5R-1, 25–30 cm (see Table 2); our preferred value for this sample is that determined by XRF. Note that almost all Leg 187 basalts have higher Zr/Nb and lower Nb/Y ratios than the average N-MORB composition of Sun and McDonough [1989], suggesting greater source depletion, yet La/Yb ratios are generally higher than average N-MORB, suggesting the opposite.

isotope ratio to the limestone from Site 1153 and marine sediments in general [Ben Othman et al., 1989; Hemming and McLennan, 2001]. Hand-picked, acid-leached glass from the same sample as the analyzed palagonite is virtually indistinguish-

able in its trace element pattern from the crystallised pillow interior, with the exception of small positive Pb and U anomalies in the glass (Figure 9b). It could be assumed from this that the REE have been mobilized and lost during alteration of the glass to

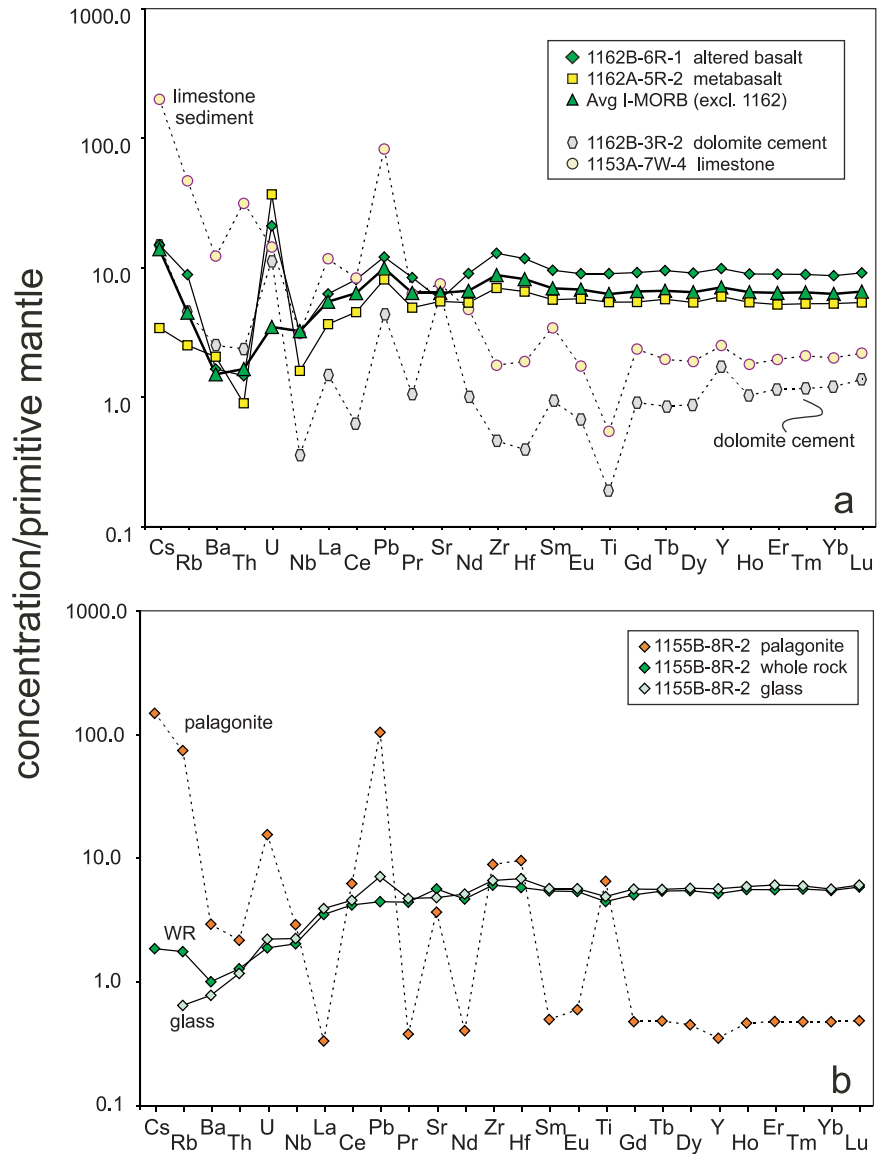


Figure 9. Extended trace element plots for (a) altered basalts and sediments from Leg 187 and (b) glass, whole rock and palagonite from Sample 1155B-8R-2, 5–9cm. Normalising values of Sun and McDonough [1989].

palagonite, whereas the HFSE (and Sr?) are largely unaffected by alteration. However, isotopic data confirm that even Sr, Nd, and Hf have been modified to some extent, as $^{143}\text{Nd}/^{144}\text{Nd}$ and $^{176}\text{Hf}/^{177}\text{Hf}$ ratios are slightly lower and $^{87}\text{Sr}/^{86}\text{Sr}$ higher in the palagonite than in the associated glass or whole rock (Table 1).

[31] In contrast, glass and whole rock analyses are isotopically identical to one another within analytical uncertainty (Table 1). This indicates

that alteration of glass is largely restricted to zones of palagonite formation. However, in most cases, it requires the presence of less than 1% palagonite to have a measurable effect on the Pb isotope composition of a glass sample, so considerable care must be observed in the picking and cleaning of the glass. The similarity between our glass and whole rock analyses also means that either (1) the leaching procedure we used has effectively removed any secondary effects for those whole rock samples that are only mildly

altered or (2) the Pb isotope ratios were not significantly affected by alteration to begin with. Neither conclusion is likely to be true for the more thoroughly altered rocks from Site 1162, however, as indicated by the scatter in their Pb isotope ratios relative to other Leg 187 basalts (Figure 3).

6. Discussion

6.1. Nd-Hf as a Viable Discriminant Between Indian MORB and Pacific MORB

[32] The data presented in Figure 4 show that $\epsilon_{\text{Hf}} - \epsilon_{\text{Nd}}$ is nearly as effective as Pb isotope space at discriminating between Indian and Pacific MORB isotopic domains. In this diagram, Indian MORB is displaced to lower Nd and higher Hf isotope ratios compared to Pacific MORB. As with the Pb isotope plot, there is very little overlap between the two mantle types (compare Figures 2b and 4b). However, much of the ridge system within the Indian Ocean is unknown in terms of its Hf isotope composition, and the small amount of data available suggest that the Southwest Indian Ridge (SWIR) may present a more complicated picture, containing Atlantic/Pacific-type mantle as well as Indian MORB (Figure 4a). Clearly, detailed sampling and analysis will be required to address this question.

[33] Our new data confirm one of the previously assumed advantages of Nd-Hf isotope systematics, i.e., its resistance to alteration. Trace element data show that U and Pb are highly mobile during alteration (Figures 7 and 9), which can have serious implications for interpretation of Pb isotopes in older rocks. It has previously been assumed that Pb is leached from, but not added to, MORB during alteration [Rehkämper and Hofmann, 1997], but the trace element patterns in Figures 7 and 9 suggest otherwise. This is particularly true for alteration of basaltic glass: palagonite is strongly enriched in U and Pb relative to other elements (Figure 9b). Furthermore, uncertainty in the U/Pb ratio and timing of the U \pm Pb enrichment can make it difficult to confidently apply an age correction to the data in

some cases. For example, the age-corrected $^{206}\text{Pb}/^{204}\text{Pb}$ value of the microgabbro (sample 1162A-5R-1, 25–30 cm) differs from the measured value by 3%, even after extensive leaching, a difference large enough to change the inferred mantle provenance (see Table 1). In contrast, leached and unleached $^{143}\text{Nd}/^{144}\text{Nd}$ values for this sample are indistinguishable (Table 1), and both measured and age-corrected values yield the same mantle provenance.

[34] Nonetheless, combining the information from Pb, Nd, and Hf isotopes allows us to put some constraints on the timing of alteration in this case. Knowing from the Nd-Hf systematics that the sample is clearly of Indian MORB provenance, and if we assume the corrected $^{206}\text{Pb}/^{204}\text{Pb}$ value should be similar to that of unaltered basalts from this zone, we can estimate that U enrichment must have occurred at least 10–12 m.y. after formation.

[35] Another advantage of Nd-Hf isotope systematics is that crystalline whole rocks can be used with confidence; precious hand-picked glasses are not necessary, as crystalline whole rock material yields the same result. Compare, for example, the compositions of glass and whole rock pairs for samples D1-2, D7-3, D7-7, and 1155B-8R2, 5–9 (Table 1), which do not differ outside of the analytical uncertainty of the data (see appendix B). Leached and unleached powders are similarly indistinguishable (see data for sample 1155A-7R-1, 16–19 cm, Table 1).

[36] Finally, ϵ_{Nd} versus ϵ_{Hf} may be uniquely well suited to address problems of mantle provenance in convergent margin settings [Pearce *et al.*, 1999; Kempton *et al.*, 2001b]. This is because Pb is highly nonconservative, so its composition in arc rocks is overwhelmingly dominated by the subducted component [Pearce and Peate, 1995]. In contrast, Hf and Nd are usually more conservative during subduction processes (just small corrections for subduction-addition being required; Pearce and Kempton [2001]); they, therefore, provide a more accurate reflection of the original mantle wedge isotopic composition [Pearce *et al.*, 1999; Kempton *et al.*, 2001b].

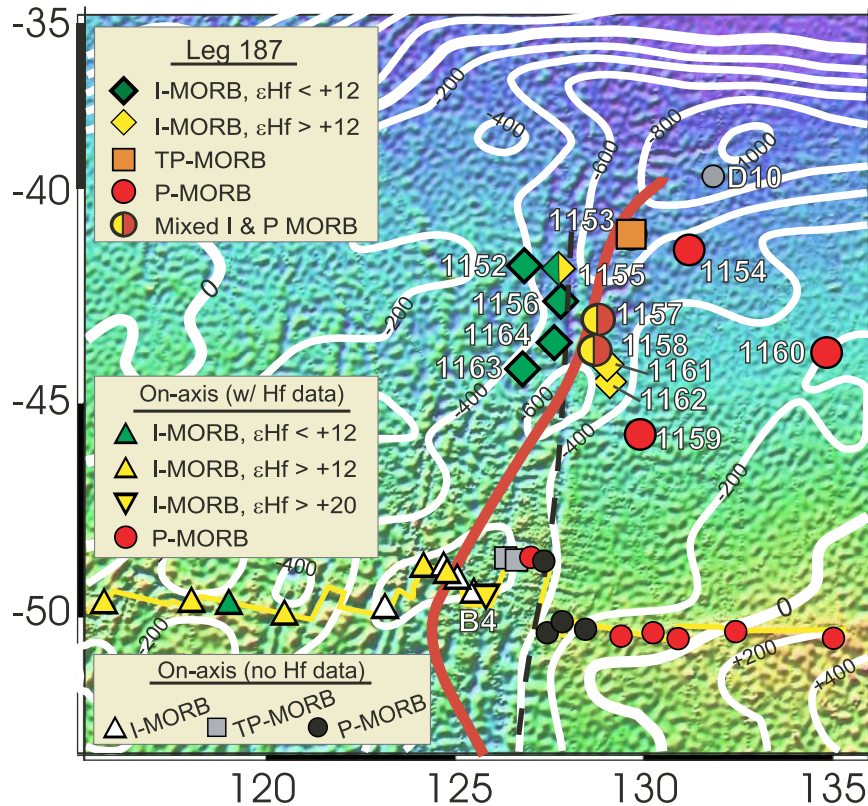


Figure 10. Color shaded relief map of modelled topography from *Smith and Sandwell* [1997] with the position of the residual depth anomaly marked by white contour lines (contour interval = 200 m) [from *Marks et al.* 1990]; approximate axis of the residual depth anomaly emphasised by the dark red line. The 127°E fracture zone between Zones B5 and A highlighted by the black dashed line. Provenance for basalts from each Leg 187 drill site indicated by large colored symbols. Smaller symbols indicate provenance of on-axis samples; data from *Klein et al.* [1988] and *Pyle et al.* [1992]. On-axis samples for which Hf isotope data are available [this study; *Salters*, 1996] distinguished by colored symbols. DR10 indicates location of Dredge Site 10 from *Lanyon et al.* [1995].

6.2. Implications for the Tectonics and Geodynamics of the AAD

[37] *Palmer et al.* [1993] summarized the various models for mantle dynamics beneath the AAD, and these include (1) convergent convective flow with asthenospheric downwelling [*Weissel and Hayes*, 1974; *Klein et al.*, 1988; *Marks et al.*, 1991], (2) cold mantle (i.e., because the mantle is cold and more viscous than normal, return flow due to plate separation draws normal asthenosphere along axis from the east and west of the AAD) [*Forsyth et al.*, 1987], (3) the shrinking Pacific plate model in which shallow mantle outflow from the shrinking Pacific plate meets a similar stream flowing out of the Indian ocean due to return flow from subduction zones

[*Alvarez*, 1990], and (4) plume-driven flow (i.e., westward flow from the Tasmanid and Balleny hot spots meets eastward flow from the Amsterdam hot spot) [*Marks et al.*, 1991]. The new Hf-Nd-Pb data presented here place some useful constraints on the viability of these various models.

6.2.1. No Evidence for Rapid Migration of Pacific Mantle

[38] The isotopic affinities of the Leg 187 drill sites are summarized in Figure 10 relative to the trace of the residual depth anomaly and the fracture zone boundary between Zones A and B at 127°E. The basalts along the western margin of the residual depth maximum are derived predominantly from

Indian mantle, but Pacific mantle is clearly present near the eastern margin from as early as 28 Ma (e.g., Site 1154). Transitional-Pacific basalts (i.e., mixtures between Indian and Pacific MORB) are located east of the midpoint of the residual depth anomaly at Site 1153. Slightly older (30 Ma) transitional basalts are reported from dredge site D10, which is located less than ~ 200 km NE of Site 1153 [Lanyon *et al.*, 1995]. Similarly, Transitional-Pacific basalts are erupting today in Zone B5 [Pyle *et al.*, 1995], which is also located east of the maximum in the depth anomaly (Figure 1). Thus transitional basalts tend to occur near to (but east of) the middle of the residual depth anomaly.

[39] Transitional-Pacific basalts are not observed between 14 and 28 Ma, but basalts derived from both Indian and Pacific mantle domains have been sampled at Sites 1157 and 1158 (22.5 and 21 Ma, respectively), and within the same hole at Hole 1157A. The significance of the inter-stratification of Indian MORB and Pacific MORB is unclear, as the deposits from both of these sites are interpreted as talus or rubble (see appendix A), so the material is not in situ and not necessarily all of the same age. However, transport distances in this environment are presumably short, so the observation still implies close proximity of the two mantle domains.

[40] Thus, although temporal variations in isotopic composition can be discerned relative to the fracture zone boundary between Zones A and B at 127°E, the distribution of different compositional groups appears to have remained much the same relative to the position of the residual depth anomaly for the past 30 m.y (Figure 10). This observation makes it difficult to support models requiring rapid influx of Pacific mantle from the east after separation of Australia from Antarctica. It has been argued that Pacific mantle would have been unable to migrate westward in the uppermost mantle until after Antarctica separated from the South Tasman Rise, which first took place between 36 and 43 m.y. ago [Royer and Sandwell, 1989]. If Pacific mantle began migrating westward at that time, unrealistically high migration rates (25–50 cm/yr) would be required for it to reach Site 1153 by 28 Ma (recall that the migration rate estimated from

the V shape of the residual depth anomaly is only ~ 1.5 cm/yr [Christie *et al.*, 1998]). We can therefore discount the “shrinking Pacific plate” model [Alvarez, 1990] and the “rapid migration” model [Christie *et al.*, 1998]. This conclusion is consistent with that of Christie *et al.* [2001], Russo *et al.* [2000], and Pyle *et al.* [2000] who suggested that the long-term (0–100 m.y.), basin-scale migration of the boundary between Indian and Pacific mantle is related to the mantle dynamics that have created and maintain the depth anomaly.

6.2.2. Lateral Flow Models

[41] Elimination of the “rapid migration” hypothesis still leaves unresolved the problem of how the isotopic boundary is maintained. Lateral flow of asthenosphere along the ridge axis, whether in response to plate separation (i.e., the cold mantle model of Forsyth *et al.* [1987]), plume-driven flow [Marks *et al.*, 1991] or mantle-scale, convergent convective flow [Klein *et al.*, 1988] via a “slow-migration” model [Pyle *et al.*, 1992; Christie *et al.*, 1998], is difficult to evaluate on the basis of geochemistry because so little data exist for the compositional heterogeneity east and west of the AAD. However, as pointed out by Christie *et al.* [1998], adiabatic melting seems improbable if the asthenosphere is actually downwelling. Similarly, numerical modeling shows that the thermal structure beneath the AAD [Kuo, 1993] is consistent with a state of retarded upwelling rather than net downwelling.

[42] Lanyon *et al.* [1995] discounted plume-driven flow as a means of maintaining the geodynamics of the AAD, because zero-age basalts from Zone A show no evidence for contamination of their source by the HIMU Balleny and Scott plumes further east. Our new data for Leg 187 basalts confirm this interpretation (Figure 11) and further indicate that the isotopic composition of the mantle source feeding Zone A has changed little over the past 28 m.y (Figures 3, 5, and 7). Similarly, there is no evidence for an increase with time in a Kerguelen- or Amsterdam/St. Paul-like plume component among basalts derived from Indian mantle. In fact, Nd-Hf isotopes suggest the opposite (Figures 4 and 5). SEIR basalts with the strongest plume signa-

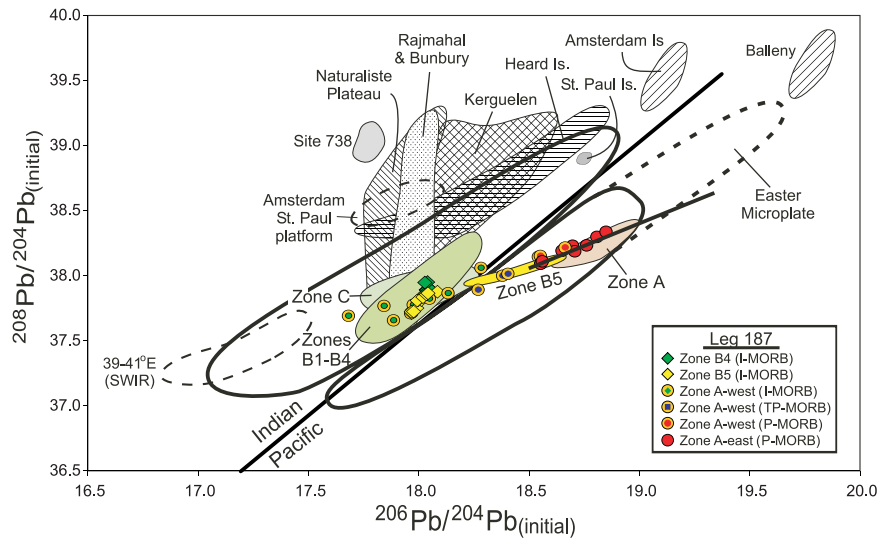


Figure 11. Plot of $^{208}\text{Pb}/^{204}\text{Pb}$ versus $^{206}\text{Pb}/^{204}\text{Pb}$ comparing AAD basalts [this study, Klein *et al.*, 1988, 1991; Pyle *et al.*, 1992] with fields for Kerguelen [Weis *et al.*, 1993; Yang *et al.*, 1998], Naturaliste Plateau and Site 738 [Mahoney *et al.*, 1995], Heard Island [Barling *et al.*, 1994], 39°–41°E SWIR [Mahoney *et al.*, 1992], St. Paul Island [Frey and Weis, 1995], Balleny Island [Lanyon *et al.*, 1993], Bunbury [Frey *et al.*, 1996] and Rajmahal basalts [Kent *et al.*, 1997]. The radiogenic end of the Pacific MORB array (i.e., $^{206}\text{Pb}/^{204}\text{Pb} > \sim 19$, indicated by dashed line) is defined by lavas from the Easter Microplate, which are known to have plume affinities. Solid black line through Pacific MORB samples from the AAD is a regression line for both on- and off-axis samples showing the trend of the data is not toward the composition of the Balleny plume.

tures, i.e., D2 and D3 from the St. Paul-Amsterdam platform [Chauvel and Blichert-Toft, 2002], have very low ϵNd and ϵHf values, plotting well down the OIB array (Figure 4). In contrast, on-axis basalts derived from Indian mantle have higher ϵHf values than 17–25 Ma Indian MORBs recovered during Leg 187 (Figure 5), i.e., they plot further away from the plume component. Thus both mantle-scale, convergent convective flow (plus downwelling) and plume-driven flow appear to be unlikely. But, is there evidence for more local lateral flow in response to plate separation?

[43] The data summarized in Figure 10 suggest that Transitional-Pacific basalts are restricted to an area near the interface between Indian and Pacific mantle, i.e., just east of the residual depth anomaly maximum. Similarly, between 14 and 28 Ma, Indian MORBs with high Hf isotope ratios (i.e., $\epsilon\text{Hf} > +12$) are found near to, and predominantly east of, the depth maximum; but low ϵHf basalts ($\epsilon\text{Hf} < +12$) are found almost exclusively west of the residual depth anomaly maximum. The range of ϵHf values across Zones B and C today is even more extreme. Indeed, although most of the on-axis

basalts from Zones C and B1-B3 have ϵHf values between +12 to +14.5, some of the most radiogenic Hf isotope compositions recorded for MORB are observed in Zone B4: $^{176}\text{Hf}/^{177}\text{Hf}$ of 0.2834 to 0.2836, which is equivalent to ϵHf values of +22 to +29 [Salters, 1996; Hanan *et al.*, 2000]. In other words, for a given time line over the past 30 m.y., the Indian MORBs furthest east within the AAD tend to have the highest ϵHf values (Figure 10), and Transitional-Pacific MORBs (i.e., basalts whose source region encompasses the isotopic boundary) are found near to, or east of, such basalts.

[44] One interpretation of this observation is that lateral flow toward the interface has been limited in extent. Even at a modest eastward flow rate of 1.5 cm/yr, over the time span investigated by Leg 187, the high- ϵHf Indian mantle (i.e., $\epsilon\text{Hf} > +12$) feeding Zone A-west should have been entirely replaced by low- ϵHf Indian mantle (i.e., $\epsilon\text{Hf} < +12$) from Zone B. One assumption implicit in this interpretation is that Indian mantle is homogeneous and that the isotopic composition does not change as a result of progressive depletion during lateral flow toward the interface. Alternatively, if Indian mantle

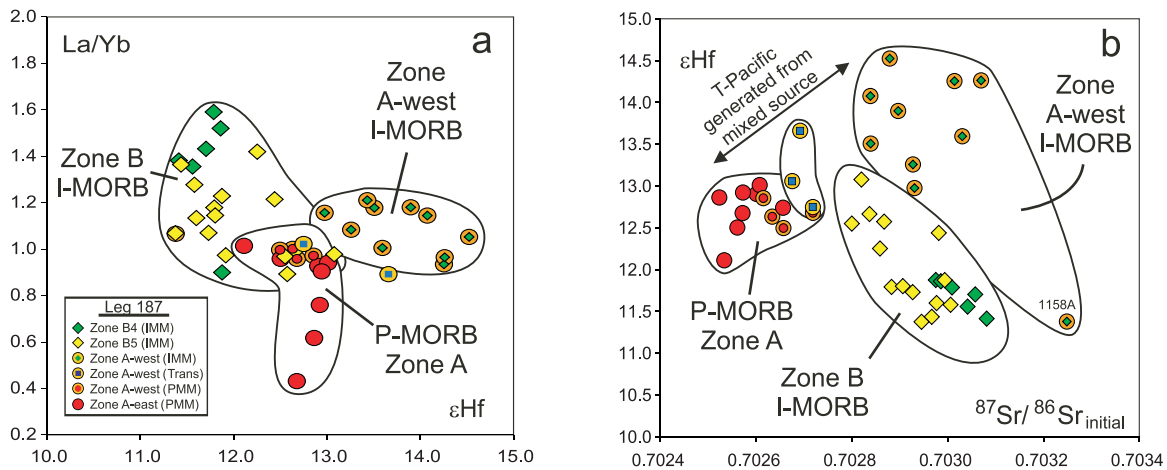


Figure 12. (a) Plot of La/Yb versus ϵHf . (b) Plot of ϵHf versus $^{87}\text{Sr}/^{86}\text{Sr}_{\text{initial}}$. Both diagrams demonstrate that high- ϵHf Indian MORBs from Zone A-west cannot represent the depleted end-member for Indian MORB beneath Zone B between 14 and 28 Ma. Figure 12b also highlights the fact that Transitional-Pacific MORBs are generated as mixtures of Pacific mantle and high- ϵHf Indian mantle from Zone A-west.

is heterogeneous, consisting of enriched streaks in a more depleted matrix, the enriched streaks could be progressively stripped out (because of their lower melting temperature) as the asthenosphere migrates eastward, leaving the most depleted compositions at the interface between Indian and Pacific mantle.

[45] The slightly more depleted trace element signatures of Indian MORBs from Zone A-west relative to those from Zone B (Figure 8) would appear to support this idea. However, progressive depletion of a heterogeneous Indian MORB source during lateral flow is unlikely for several reasons. Although the highest La/Yb ratios are found among Indian MORBs from Zone B, more depleted basalts from this zone have La/Yb ratios that overlap those of Zone A-west basalts; yet there is almost no overlap in ϵHf isotope composition and no systematic variation between the two groups (Figure 12a). Similarly, Indian MORBs from Zone B show a strong negative correlation between $^{87}\text{Sr}/^{86}\text{Sr}$ and ϵHf (Figure 12b); yet basalts from Zone A-west do not lie along an extension of this array, having higher $^{87}\text{Sr}/^{86}\text{Sr}$ for a given ϵHf . This is true, even if we exclude the highly altered samples from Site 1162. These observations indicate that Zone A-west basalts do not represent the depleted end-member of a heterogeneous Indian MORB source like that feeding Zone B.

[46] Finally, we note that the geographic distribution of Indian MORBs with high ϵHf values has expanded westward with time along the current ridge axis rather than contracted, as might be expected by lateral flow toward the interface (Figure 10). Therefore, although we cannot fully discount a lateral flow model as a mechanism for maintaining the unusual dynamics of the AAD, the isotopic and trace element data for Leg 187 do not readily support it. We therefore discuss an alternative explanation in section 6.2.3.

6.2.3. Stagnated Subducted Slab Model

[47] *Gurnis et al.* [1998] proposed that the unusual dynamics of the AAD are due to the Australian and Antarctic plates having moved eastward over an old subduction zone, which existed between the Pacific plate and the eastern margin of Gondwanaland up until the Early Cretaceous and had probably been active off the combined margin of Australia and Antarctica since the Cambrian [Unrug, 1996]. During the Late Cretaceous the position of convergence passed under the eastern interior of Australia and is located today beneath the AAD. *Gurnis et al.* [1998] note that the thinned crust (i.e., the residual depth anomaly), which characterizes the AAD today, does not extend uniformly north-south. Instead, crustal thickness reduces significantly after ~ 20 Ma, from only a few hundred meters less than normal 10 m.y after

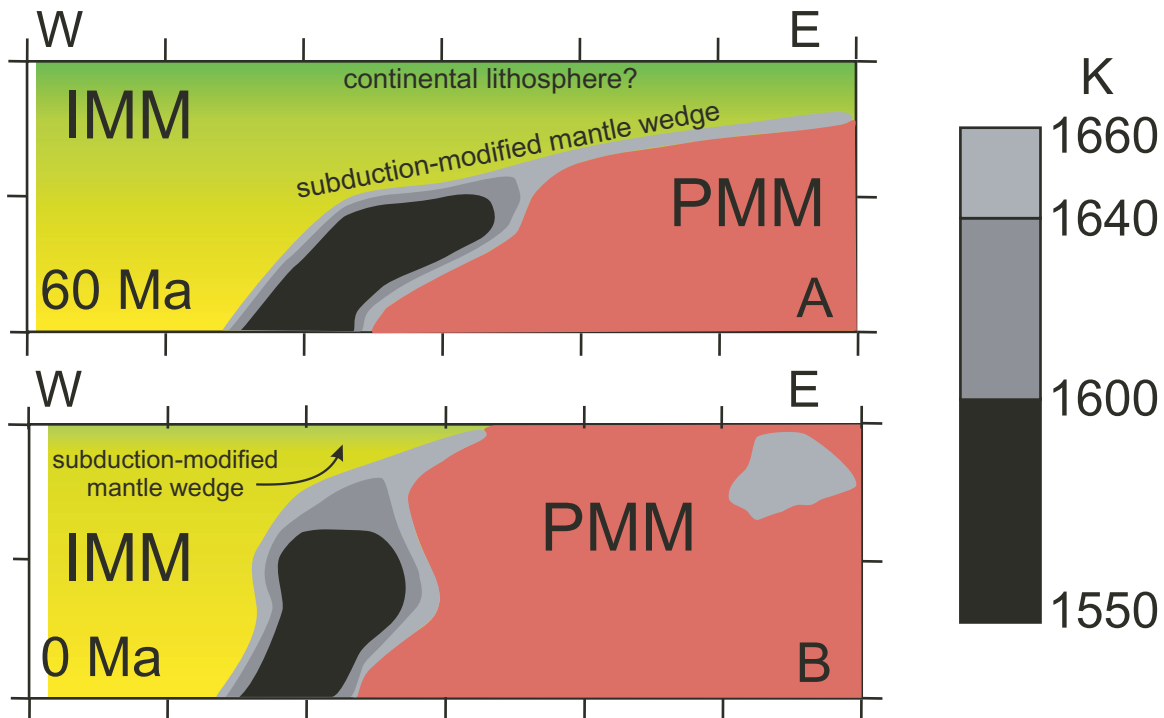


Figure 13. Schematic cross-section of the mantle at (a) 60 Ma and (b) 0 Ma, based on the model of *Gurnis et al.* [1998]. Precise locations of the cross-sections are shown in *Gurnis et al.* [1998], but their approximate location is from 115° to 150°E. At 60 Ma the cross-section lies beneath the Australian continent; at 0 Ma the cross-section lies underneath the SEIR. The scale at the right shows model temperatures for the subducted slab in K. Tick marks indicate intervals of 500 km.

rifting to 1 km thinner at the present time. They argue that the thinned crust is caused by the upwelling of a portion of old slab that partially stagnated in the transition zone beneath the ridge. The timing of the onset of thinner crust corresponds to the time it took the slab to be drawn up from the transition zone, starting at ~45 Ma when rifting between Australia and Antarctica accelerated. Thus the apparent migration of the residual depth anomaly and the isotopic boundary between Indian and Pacific mantle are primarily due to the eastward motion of the Australian and Antarctic plates, relative to the hot spot reference frame, moving progressively over a stagnated slab oriented roughly orthogonal to the ridge axis.

[48] The *Gurnis et al.* [1998] model for the mantle dynamics of the AAD is attractive because it not only appears to match the gross geophysical and geochemical features of the present-day SEIR but also predicts the link between the residual depth anomaly and the isotopic boundary demonstrated

by the data from Leg 187 basalts. Because the slab acts as a physical barrier between the Indian and Pacific mantle domains, it also explains why transitional and “mixed” domain sites are relatively uncommon and restricted in geographic occurrence.

[49] However, geochemical characteristics commonly associated with subduction zone lavas, such as strong relative depletion in the HFSE, are lacking. In fact, some HFSE are high relative to adjacent elements in extended trace element patterns (Figure 7). On the other hand, *Graham et al.* [2001] found that $^3\text{He}/^4\text{He}$ ratios for basalts from the AAD are as low as 6.2 (R/R_A), and are among the lowest values yet observed in MORB away from the influence of subduction zones.

[50] Neither of these observations unambiguously proves or disproves the model of *Gurnis et al.* [1998]. However, the absence of strong geochemical signatures associated with subduction may be explained if the slab and its sediment cover are too

deep to chemically modify the MORB-source reservoir, but shallow enough to exert an influence on the thermal and convective regime of the mantle beneath the AAD. In addition, the subducted slab and sediment are unlikely to be the source of fluids that could metasomatise the overlying mantle, because they have already been significantly dehydrated and/or partially melted as a result of passing through a subduction zone. Nonetheless, the dynamics of the stagnated subducted slab model appear to be able to explain the distribution of isotopic compositions within the AAD more readily than lateral flow along the ridge axis.

[51] As shown in Figure 12, the high- ϵ Hf Indian mantle feeding Zone A-west is distinct from the Indian mantle feeding Zone B (between 14 and 28 Ma) as well as from Pacific mantle. Its geographic distribution also appears to have increased over time, as Zones B and C are almost exclusively fed by high- ϵ Hf Indian MORB today (Figure 10). These two observations are explicable if the high- ϵ Hf mantle originates from a location deeper in the mantle than the low- ϵ Hf mantle feeding Zones B4 and B5 between 17 and 25 Ma. This is shown schematically in Figure 13. Figure 13a shows a cross-section of the mantle at 60 Ma based on the model of *Gurnis et al.* [1998]. This is ~ 30 m.y. after cessation of subduction off eastern Australia, but 10–15 m.y. prior to separation of Australia from Antarctica. At this time the slab was located beneath the Australian continent. The mantle overlying the slab would have been a mixture of subduction-modified mantle wedge and pre-existing Indian MORB mantle; Pacific mantle is separated from the overlying Indian mantle by the subducting (but stagnated) slab. As Australia and Antarctica separate, the stagnated slab gradually upwells, forcing ahead of it the subduction-modified mantle that overlies it. By the present-day (Figure 13b), the model predicts that this upwelled material dominates the region of MORB-source mantle beneath the ridge. This model also explains why transitional basalts tend to be mixtures between Pacific MORB and high- ϵ Hf Indian MORB only, as most of the low- ϵ Hf Indian mantle is displaced before Pacific mantle arrives beneath the ridge by the high- ϵ Hf Indian MORB ascending

ahead of the upwelling slab. This scenario begs the question of why the deeper, subduction-modified mantle being pushed ahead of the upwelling slab should have a high ϵ Hf isotope signature, and we offer a possible explanation for this in section 6.3.

6.3. Nd-Hf Isotope Systematics and the Origin of Indian MORB-Source Mantle

[52] Most models for the origin of Indian MORB involve contamination of a “normal” depleted mantle by a distinctly enriched material, the most favored being (1) recycled oceanic crust plus pelagic sediments [*Rehkämper and Hofmann*, 1997], (2) mantle plumes [*Storey et al.*, 1989; *Mahoney et al.*, 1992], and (3) subcontinental lithosphere [*Mahoney et al.*, 1995, 1996]. *Rehkämper and Hofmann* [1997] argue that because all of the known mantle plumes in the Indian Ocean have $^{206}\text{Pb}/^{204}\text{Pb} > 18$, contamination of depleted mantle by this material cannot account for the full spectrum of Indian MORB compositions. Similarly, they discounted delamination of continental lithosphere because the low trace element concentrations expected in lithospheric mantle would require unrealistically large volumes of material to be delaminated in order to effect a significant change in the underlying asthenosphere. Instead, these authors showed through quantitative mixing models that recycling of an old, compositionally heterogeneous component could explain the range of Sr, Nd, and Pb isotope compositions for Indian MORBs. Their model predicts that the predominant recycled component is ancient (1.5 Ga) altered ocean crust, with pelagic sediment comprising less than 10% of the contaminant.

[53] *Chauvel and Blichert-Toft* [2002] suggest that the recycling model is consistent with the Hf-Nd isotope systematics of Indian MORB because ancient pelagic sediments have very low ϵ Hf and ϵ Nd as well as high Nd/Hf ratios relative to MORB [*Patchett et al.*, 1984; *Vervoort et al.*, 1999]. Thus mixing curves tend to be broadly concave downward. This means that over small degrees of mixing, addition of pelagic sediments to a Pacific-like mantle should reduce the Nd isotope ratios, while leaving the Hf isotope ratios largely unchanged, thereby

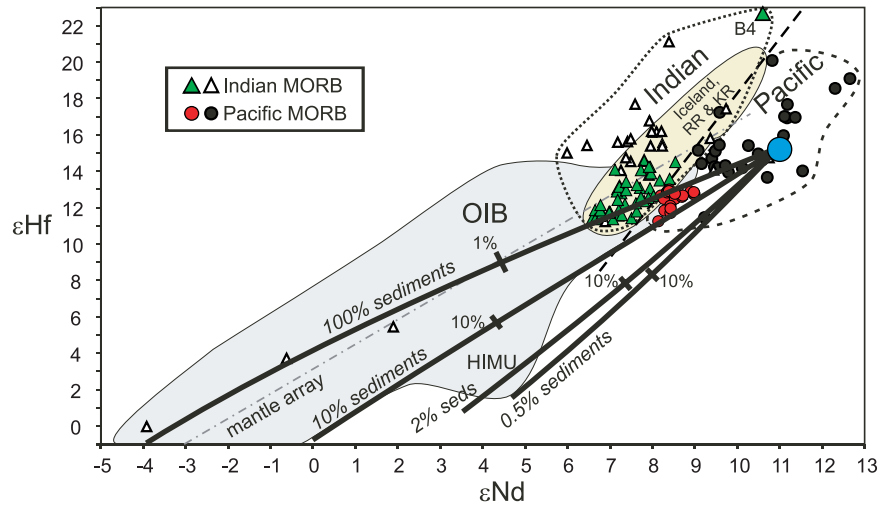


Figure 14. Plot of ϵ_{Hf} versus ϵ_{Nd} showing results of mixing calculations for the contamination model. The thick black lines show the consequences of adding four potential recycled components to the assumed depleted mantle composition (large blue dot). Three of the recycled components are mixtures of 1.5 Ga altered ocean crust with 10%, 2% and 0.5% ancient pelagic sediment; one is for addition of 100% pelagic sediment. Tick mark on the curves involving ocean crust is for 10% recycled material; tick mark on the curve for 100% sediment indicates just 1% recycled material. Data sources as in Figures 4 and 5. Colored symbols denote Indian and Pacific MORBs from the AAD. See Table 3 for model parameters.

accounting for the offset of Indian MORB from Pacific MORB in Hf-Nd isotope space (Figure 4).

[54] However, implicit in this model is that (1) the mixing is relatively recent or the Indian MORB array would shift downward as well as to the left of the Pacific MORB array with time in response to lower Sm/Nd and Lu/Hf ratios acquired through addition of the enriched component, and (2) there must be more than one (and probably a range) of depleted compositions within the mantle prior to sediment addition in order to account for the full range of Hf isotope compositions observed for Indian MORBs.

[55] We demonstrate this quantitatively in Figure 14, where we extrapolate the modeling approach used by *Rehkämper and Hofmann* [1997] to $\epsilon_{\text{Hf}} - \epsilon_{\text{Nd}}$ isotope space. Model parameters are summarized in Table 3. In the model of *Rehkämper and Hofmann* [1997], most of the Indian MORB field is described by 0–10% mixing of ancient altered oceanic crust, plus a pelagic sediment component of less than ~5%. Only Indian MORBs with unusually low $^{206}\text{Pb}/^{204}\text{Pb}$ (i.e., less than ~17.5) require a significantly greater proportion (~10%) of pelagic sediment. However, Figure 14 shows that in ϵ_{Nd} versus

ϵ_{Hf} space, model curves for mixing between a single depleted mantle composition and a range of enriched components containing less than 10% pelagic sediment do not pass into the Indian MORB field. Even if we assume mixing of 100% pelagic sediment, the mixing curves are only modestly concave downward. This is because the Nd/Hf ratio of average subducted sediment (e.g., GLOSS; *Plank and Langmuir* [1998]) is only ~1.5 times higher than that of depleted mantle, even though trace element abundances are greater by more than an order of magnitude (see Table 3). Furthermore, this Nd/Hf ratio is probably a maximum because fluids derived from sediments in subduction zones have higher Nd/Hf ratios than the bulk sediments [*Pearce et al.*, 1999]; thus the residues from this process (i.e., the material most likely to be subducted) would have Nd/Hf ratios that are even lower than the starting material. In the unlikely event that the Nd/Hf ratio of the ancient pelagic sediment component is higher than GLOSS, the curvature of the mixing curves would be greater, but this would still fail to explain the wide range of ϵ_{Hf} values among Indian MORBs. As shown in Figure 14, because the Indian and Pacific MORB fields are roughly parallel and because the Indian MORB field extends to very high ϵ_{Hf} values

Table 3. Composition of the End Members Involved in the Contamination Model^a

	1.5Ga N-MORB	1.5Ga altered N-MORB	1.5 Ga pelagic sediment	Present-day depleted mantle
Nd	7.3	7.3	27	0.951
Sm	2.63	2.63	5.78	0.348
Hf	2.05	2.05	4.06	0.228
Lu	0.455	0.455	0.413	0.064
¹⁴⁷ Sm/ ¹⁴⁴ Nd	0.218	<i>0.196</i>	0.129	0.221
¹⁷⁶ Lu/ ¹⁷⁷ Hf	0.032	<i>0.027</i>	0.014	0.038
Lu/Hf	0.22	0.22	0.10	0.28
Nd/Hf	3.56	3.56	6.65	4.17
<i>Present day isotopic composition</i>				
¹⁴³ Nd/ ¹⁴⁴ Nd	0.5132	0.5129	0.5117	0.5132
¹⁷⁶ Hf/ ¹⁷⁷ Hf	0.28297	0.28282	0.28205	0.28320
<i>Isotopic compositions at 1.5 Ga</i>				
¹⁴³ Nd/ ¹⁴⁴ Nd	0.51102	0.51102	0.51040	0.51102
¹⁷⁶ Hf/ ¹⁷⁷ Hf	0.28203	0.28203	0.28163	0.28203

^aThe composition of N-MORB is from *Sun and McDonough* [1989]; depleted mantle values from *Chauvel and Blichert-Toft* [2002]; pelagic sediment composition from *Plank and Langmuir* [1998]. Nd isotope composition of depleted mantle, N-MORB and pelagic sediment from *Rehkämper and Hofmann*, 1997]; Hf isotope compositions for altered N-MORB and depleted have been estimated based on data in Figure 4 to correspond to the assumed Nd values; value for pelagic sediment estimated from data in *Vervoort et al.* [1999]. Parent/daughter ratios for the isotopic systems were calculated for the listed trace element and isotope data, except for altered N-MORB. In this case, we followed the rationale of *Rehkämper and Hofmann* [1997] and derived the parent/daughter ratios (shown in italic) from the present-day isotope systematics of HIMU basalts.

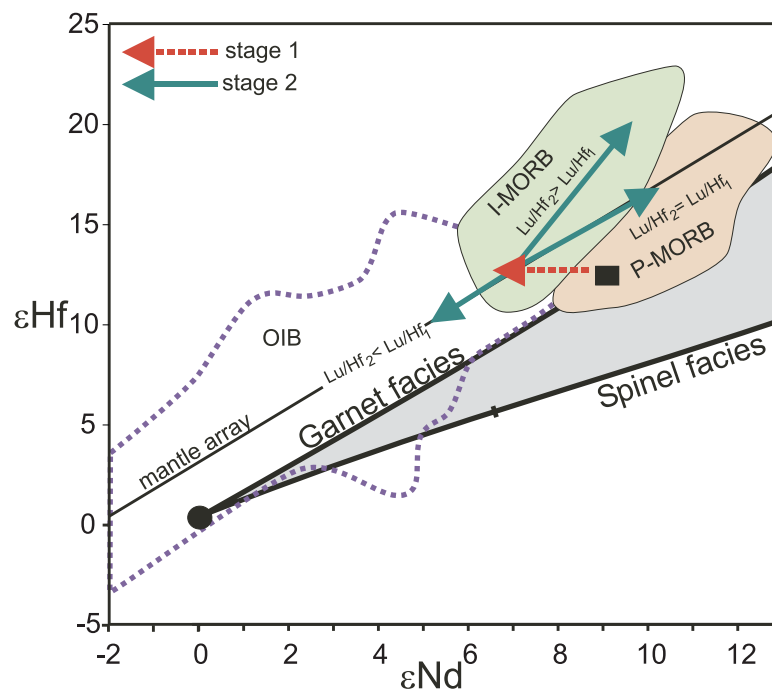


Figure 15. Plot of ϵHf versus ϵNd showing conceptual model for the consequences of subduction-modification on mantle evolution curves. Heavy black curves labeled garnet facies and spinel facies indicate the path of evolution for depleted mantle formed by non-modal fractional melting at 2 Ga (see *Kempton et al.* [2000] for details of calculations). Note that if partial melting involves 1–2% trapped melt, the curves shift to slightly steeper trajectories: garnet facies melting with 0% trapped melt follows a similar trajectory to spinel facies melting with ~2% trapped melt. Lu/Hf_1 represents the Lu/Hf ratio of the depleted mantle prior to recycling of subduction-modified mantle; Lu/Hf_2 is the ratio after recycling of subduction-modified mantle.

(> +22 [Hanan *et al.*, 2000], the ϵ_{Hf} value of the depleted mantle starting composition would have to be considerably more radiogenic than is currently observed for either Pacific or Atlantic MORB in order to account for the complete range of the Indian MORB field. We consider this unlikely, not least because Pacific mantle from the Southern Hemisphere has lower ϵ_{Nd} [Vlastelic *et al.*, 1999] and ϵ_{Hf} (Figure 4) on average than that of the Northern Hemisphere.

[56] Clearly, in order to explain the Hf-Nd isotope systematics, we must look for a mechanism that involves not only enrichment but also relative depletion of the mantle source. Subduction-modification of the mantle is one such mechanism, and one that is consistent with the geologic history of the region. We know that subduction occurred periodically off the east coast of Gondwana from the Cambrian to the Cretaceous [Unrug, 1996]. In addition, subduction must have occurred along some of the suture zones between the cratonic blocks involved in the assembly of Gondwana during the Precambrian [Fitzsimons, 2000]. This means that a significant proportion of material in the upper mantle beneath Gondwana could have been processed in the mantle wedge of a subduction zone.

[57] The consequences of this hypothesis, in terms of Hf-Nd isotope systematics, are depicted qualitatively in Figure 15. During stage 1, dewatering of the slab and/or partial melting of subducted sediments enrich at least some portions of the mantle wedge in REE relative to the HFSE. Assuming that the fluids and/or melts passing through the mantle wedge are derived from sediments that have been shed from old continental crust, the Nd isotope composition of the wedge probably decreases due to equilibration with the metasomatic fluids. Most of the incompatible elements added to the wedge during this process are eventually lost again through partial melting and formation of arc lavas, so the net result is that the Nd isotope ratio of the wedge decreases, while the Sm/Nd ratio either decreases slightly or remains unchanged.

[58] The $^{176}\text{Hf}/^{177}\text{Hf}$ ratio of the mantle wedge is probably less affected, because Hf is strongly

conservative during subduction processes (except in exceptional circumstances, such as continent-arc collision and ridge subduction) [Pearce *et al.*, 1999]. The Lu/Hf ratio of the mantle wedge is controlled predominantly by partial melting processes, and because Lu is more compatible than Hf, this ratio increases strongly with degree of partial melting. Hochstaedter *et al.* [2001], for example, estimate a Yb/Zr ratio of 0.14 in the residue from partial melting that formed part of the Izu-Bonin arc; from this we can infer a Lu/Hf ratio for the wedge of ~ 0.75 . Note this ratio is nearly 3 times that of the depleted mantle (i.e., ~ 0.28). In contrast, the corresponding change in Sm/Nd ratio is considerably less, i.e., ~ 0.50 for the mantle wedge residue [Hochstaedter *et al.*, 2001] versus ~ 0.37 for depleted mantle. The smaller change in the Sm/Nd ratio is in part because the partition coefficients for Sm and Nd are more similar to one another than those for Lu and Hf, but it is also because Sm and Nd are more strongly affected by metasomatic enrichment of the wedge than Hf (or Lu), which counteracts the effects of depletion due to partial melting.

[59] If metasomatism of the wedge is extensive and there is no subsequent depletion by partial melting, the Lu/Hf as well as Sm/Nd ratio can decrease. However, this scenario may have more to do with the origin of ocean island basalts [Donnelly *et al.*, 2001] than to MORB generation. We will therefore exclude it from the rest of our discussion.

[60] As a result of the compositional changes experienced by the mantle wedge during subduction processes, the isotopic evolution curve for the mantle after subduction-modification is initially shifted to lower ϵ_{Nd} (Figure 15). With time (stage 2), ingrowth of radiogenic Nd produces either an isotopic evolutionary path similar to that of the depleted mantle from which the wedge originated or one which is retarded in response to a slightly lower Sm/Nd. In contrast, Hf isotope ratios either increase along an array parallel to the normal depleted mantle or follow an even steeper evolutionary path. Note that with Lu/Hf ratios of up to 0.75, the Hf isotope compositions of most Indian MORBs could be generated in as little as ~ 150 m.y.

[61] However, the recycled mantle wedge is unlikely to be the source of significant volumes of melt because it has been so thoroughly depleted as a result of arc magmatism. It is also unlikely to remain isolated from the rest of the convecting upper mantle. Therefore whether recycling of subduction-modified mantle wedge represents a viable model for the origin of Indian mantle depends on (1) the volume of mantle wedge that has been processed, (2) the trace element contents of both the mantle wedge and the unprocessed asthenosphere into which it is returned, and (3) how thoroughly the two reservoirs are homogenised and over what timescale, none of which is well constrained. However, we note that it only requires an increase in the Lu/Hf ratio of $\sim 20\%$ (i.e., from ~ 0.28 to 0.34) to generate the range of ϵHf values shown by the majority of Indian MORBs from the AAD in ~ 500 m.y. (i.e., from $+11.5$ to $+14.5$). Similarly, if we assume an ϵHf value like that of Pacific MORB from Zone A as representative of the depleted mantle from the Southern Hemisphere (i.e., $\sim +12.5$), it only requires an increase in the Lu/Hf ratio of $\sim 8\%$ over that of depleted mantle (i.e., from ~ 0.28 to ~ 0.30) to generate most of the Indian MORB array in ~ 1.5 b.y., which is the same age as the recycled slab and sediment required by the model of *Rehkämper and Hofmann* [1997]. If we accept that a Lu/Hf ratio of 0.75 is representative of the depleted mantle wedge, it would only require about 10% of the upper mantle to have been cycled through a subduction zone in order to achieve an 8% increase in the Lu/Hf ratio of the homogenised mixture. But, is this volume of mantle wedge realistic?

[62] Assuming an average rate of arc generation of between 80 and 200 km^3/km of arc length/m.y. [*Arculus*, 1999] and an average total arc length of ~ 5000 km, between 5 and 15% of the upper mantle beneath East Gondwana could have been processed through a subduction zone in ~ 500 m.y., and as much as 45% in 1.5 b.y. Admittedly, the arcs associated with the assembly and evolution of East Gondwana are unlikely to have been active 100% of the time over 100% of their length, but even if they were only active 50% of the time, the volume of mantle involved is of the same

order of magnitude as that required by the isotope data. Furthermore, we note that Pb isotope data indicate that the upper mantle is not as convectively well mixed as previously thought (see Figure 3b and *Galer et al.* [2000]), so the mantle wedge may be only partially mixed back into the upper mantle, increasing its relative contribution on a local scale.

[63] Thus Hf isotope data for Indian MORBs are consistent with a model involving recycling of subduction-modified mantle wedge. Although it may only have been possible to sample the high- ϵHf Indian MORB within the AAD because of the unusual dynamics of the region (i.e., the upwelling stagnated slab), in other areas this material could be returned to the shallow upper mantle (i.e., the source region of MORB) via mantle plumes. An example of this mechanism may be the high- ϵHf mantle entrained as a sheath surrounding the Iceland plume in the North Atlantic [*Kempton et al.*, 2000]. Clearly, further research is required to assess whether the model proposed is generally applicable and able to explain other unusual features of Indian MORB-source mantle (i.e., Pb and Sr isotopes, Nb/U, K/Ti, Ce/Pb, etc.).

7. Summary and Conclusions

[64] Combined Nd-Hf isotope systematics can be used as an effective geochemical discriminant between Indian and Pacific mantle domains. In particular, Indian MORBs are displaced to lower ϵNd and higher ϵHf ratios compared to Pacific MORBs. Existing data suggest that, as with Pb isotope plots, there is virtually no overlap between the two mantle types: almost 95% of the data are properly discriminated by the ϵHf versus ϵNd diagram. This system has the advantage that a reliable provenance can be determined even for older, altered basalts. It may also be uniquely placed to address questions of mantle provenance in arc rocks because of the conservative nature of both Nd and Hf as compared with Pb during arc processes.

[65] The new Nd and Hf isotope data have been used to extend the characterization of the mantle domain boundary within the Australian-Antarctic

Appendix A. [The full Appendix A is available in the HTML version of the article at <http://www.g-cubed.org/>.]

Sample no	Lithology	Unit #	Type Deposit	Alteration
Site 1152: Located in Zone B4, west of the residual depth anomaly. Hole B located ~100 m N-NE of Hole A. Age ~ 25 Ma.				
1152A-1R-1, 25–29	aphyric basalt	1	talus	slight
1152A-2R-1, 51–56	aphyric basalt	1	talus	slight
1152A-4R-2, 20–24	mod plag-ol-cpx phyric basalt	2	talus	slight
1152A-6R-1, 43–49	sparse plag-ol-cpx phyric basalt	2	talus	slight
Site 1153: Located slightly east of the center of the residual depth anomaly, 225km east of 127°E Fracture zone. Seafloor terrain is chaotic with oblique lineaments, possibly indicating ridge propagation. Probably Zone A-west. Age ~ 28 Ma.				
1153A-7W-4, 5–8	lithified carbonate ooze	1	pillows	slight
1153A-7W-4, 65–69	aphyric basalt	1	pillows	slight
1153A-8R-1, 101–102	glass	1	pillows	slight
1153A-8R-1, 134–137	aphyric basalt	1	pillows	slight
Site 1154: Located in Zone A, slightly east of the locus of the residual depth anomaly, 70 km east of Site 1153. The terrain consists of NE trending en echelon grabens associated with westward rift propagation. Age ~ 28 Ma.				
1154A-2R-1, 25–27	mod plag-ol phyric	1	pillows	slight
1154A-4R-1, 13–18	mod plag-ol phyric	1	pillows	slight
1154A-9R-1, 46–50	mod plag-ol phyric	1	pillows	slight
Site 1155: Located mid-segment of Zone B5, in abyssal hill terrain, west of the locus of the residual depth anomaly. Hole B located ~200 m west of Hole A. Age ~ 24.5 Ma.				
1155A-2R-1, 29–32	sparse plag-ol phyric	1	pillows	slight
1155A-7R-1, 12–17	aphyric (sparse ol) basalt	2	talus	mod.
1155B-4R-1, 76–80	sparse plag-ol phyric	1	pillows + CCV	slight
1155B-6R-2, 140–144	sparse plag-ol phyric	1	pillows + CCV	mod.
1155B-8R-2, 5–9	mod plag-ol phyric basalt	1	pillows + CCV	slight
1155B-8R-2, 5–9	glass	1	pillows + CCV	slight
1155B-8R-2, 5–9	palagonite	1	pillows + CCV	slight
1155B-9R-2, 65–68	mod plag-ol phyric	1	pillows + CCV	slight
Site 1156: Located midway in Zone B5, west of the locus of the residual depth anomaly, 87 km S of Site 1155; Hole B 200 m N of Hole A. Age ~ 22 Ma				
1156A-2R-3, 18–24	plag-ol phyric clast in basalt-carbonate breccia	1	basalt-carbonate breccia + CCV	slight
1156A-2R-3, 135–138	mod plag-cpx phyric basalt	2	pillows	slight
1156B-2R-1, 72–82	highly plag-ol phyric	1	pillows?	slight
1156B-5R-1, 120–123	highly plag-ol phyric	1	pillows?	slight
1156B-5R-2, 26–28	highly plag-ol phyric	1	pillows?	slight
Site 1157: Located in Zone A-west, 55 km east of the 127°FZ; 230 km S of Site 1153, which is on a similar flow line and 100 km SE of Site 1156, which is the same age. Hole B 200 km west of Hole A. Age ~ 22.5 Ma				
1157A-1W-CC, 12–16	plag phyric basalt	1	rubble w/ intervals of basalt-carbonate breccia, CCV	slight
1157A-2R-1, 87–89	aphyric basalt	1	rubble w/ intervals of basalt-carbonate breccia CCV	slight
1157A-2R-1, 86–90	aphyric basalt	1	rubble w/ intervals of basalt-carbonate breccia CCV	slight
1157A-3R-1, 30–32	aphyric basalt	1	rubble w/ intervals of basalt-carbonate breccia CCV	slight
1157A-3R-1, 128–132	aphyric basalt	1	rubble w/ intervals of basalt-carbonate breccia CCV	slight
1157B-3R-1, 55–58	sparse plag-ol phyric	1	pillows	slight
1157B-6R-1, 43–46	mod plag-ol phyric	1	pillows	slight
1157B-8R-1, 12–16	mod plag-ol phyric	1	pillows	slight

Generalized summaries for each site based on *Christie et al.* [2001]. CCV, composite carbonate veins; plag, plagioclase; ol, olivine; cpx, clinopyroxene.

Discordance from on-axis to older (14–28 Ma) off-axis crust. These data show that the isotopic boundary coincides with the eastern edge of the basin-wide arcuate depth anomaly that is centered on the AAD today. This has significant implications for models of mantle flow in the region and discounts the idea that Pacific mantle has only recently arrived beneath the AAD, in agreement with the preliminary conclusions reached by *Christie et al.* [2001].

[66] Nd-Hf isotope systematics also provide the basis for a completely new model for the origin of the distinctive isotopic signature of Indian MORBs within the AAD, and possibly Indian MORBs in general. These data suggest that their mantle source originated as subduction-modified mantle wedge that was mixed back into the upper mantle beneath Gondwana. This is consistent with the model proposed by *Gurnis et al.* [1998], which explains the dynamics that maintain both the residual depth anomaly and the Indian MORB-Pacific MORB isotopic boundary as due to eastward migration of the Australian and Antarctic plates over a stagnated, but slowly upwelling, slab oriented roughly orthogonal to the ridge axis. Temporal and spatial variations in the compositions of Indian MORB basalts within the AAD can be explained by progressive displacement of low- ϵ Hf Indian MORB by high- ϵ Hf Indian MORB ascending ahead of the upwelling slab.

Appendix A: Geologic Summary of Leg 187 Drill Sites and Petrography of Analyzed Samples

[67] A brief summary of the Leg 187 drill site locations and petrographic descriptions of individual samples analyzed in this study are provided in Table A1.

Appendix B: Analytical Methods

[68] Whole rock samples were prepared for geochemistry by first removing weathered surfaces with a grinder; the samples were then crushed using a fly press, and powdered in an agate “pulviser” for

30 min. Major elements and some trace elements were determined by X-ray fluorescence (XRF) spectrometry using a Philips PW2404 spectrometer at Edinburgh University. The analytical techniques and precision are essentially the same as those described by *Fitton et al.* [1998], except for Nb. Because of the curved X-ray background around NbK α , background intensities were measured at four positions, two either side of the peak over a third-order polynomial fitted to the data. This allows a significantly more accurate estimate of the background intensities at the peak position and a corresponding improvement in analytical accuracy at low concentrations of Nb. International rock standards run with the AAD samples are listed in Table 2.

[69] All trace elements listed were analyzed on a Perkin Elmer Elan 5000 ICP-MS at the University of Cardiff, Wales. Approximately 0.1 g of unleached whole rock powder was digested in concentrated HF. After evaporation the residue was dissolved with concentrated HNO $_3$, evaporated again and dissolved in 6 cm 3 of 5M HNO $_3$. The sample solution was accurately made up to 50 cm 3 with deionized water and a 2 cm 3 aliquot was spiked with a 100 ppb solution of Re and Rh and made up to 10 cm 3 volume. A selection of international standard reference materials was used to calibrate the machine and W-2 was used as a drift monitor during analysis. Other aspects of methodology, accuracy and precision are similar to those described by *Pearce et al.* [1995]. Standard values and statistics for the AAD runs are given in Table 2. XRF analyses are used for Sc, V, Cr, Ni, Cu and Zn and ICP-MS analyses for Co, Ga, and Rb through U. XRF analyses for Rb through Nb are also reported. These show excellent correlation with the ICP-MS values except for Y, which is systematically \sim 8% higher.

[70] Sr, Nd, Pb, and Hf isotope ratios were determined at the NERC Isotope Geosciences Laboratory (NIGL). Procedures used in the analysis of Sr, Nd, and Pb isotopes are given by *Kempton* [1995] and *Royse et al.* [1998]. Whole rock powders for Sr-Nd-Pb analysis were leached in 6M HCl on a hot plate for \sim 1 hour; leached and unleached fractions of some samples were analyzed for comparison. Glass chips were prepared by first washing in Milli-Q H $_2$ O

for 30 min in an ultrasonic bath, followed by 30 min in 6M HCl (cold) in the ultrasonic bath, and finally rinsed in Milli-Q H₂O. Dissolution procedures were the same for both whole rock powders and glasses.

[71] Sr and Nd were run as the metal species on single Ta and double Re-Ta, respectively, using a Finnigan MAT 262 multicollector mass spectrometer. Sr was run in multidynamic mode and Nd in static mode. The effects of fractionation during runs were eliminated by normalizing ⁸⁶Sr/⁸⁴Sr to 0.1194; ¹⁴³Nd/¹⁴⁴Nd was normalized to a value of ¹⁴⁶Nd/¹⁴⁴Nd of 0.7219. Sample values for ⁸⁷Sr/⁸⁶Sr and ¹⁴³Nd/¹⁴⁴Nd are reported relative to accepted values of NBS 987 (0.71024) and La Jolla (0.51186), respectively. Minimum uncertainties are derived from external precision of standard measurements that over the course of analysis average 43 ppm (2σ) for ¹⁴³Nd/¹⁴⁴Nd and 26 ppm (2σ) for ⁸⁷Sr/⁸⁶Sr. Pb isotopes were analyzed on the VG P54 MC-ICP-MS, since this instrument allows us to correct for mass fractionation during the run using the Tl-doping method. We have used a ²⁰⁵Tl/²⁰³Tl value of 2.388, which was determined empirically by cross calibration with NBS 981. All Pb isotope ratios have been corrected relative to the NBS 981 composition of *Todt et al.* [1996]. Based on repeated runs of NBS 981, the reproducibility of whole rock Pb isotope measurements is better than ±0.01% (2σ).

[72] Procedures for Hf follow those described by *Kempton et al.* [2001a]. Whole rock powders for Hf analysis were unleached, although leached and unleached pairs were analyzed in some cases for comparison. Within-run standard error for Hf isotope measurements is normally less than 22 ppm (2σ). Minimum uncertainties are derived from external precision of standard measurements, which average 42 ppm (2σ). Replicate analysis of our internal rock standard, pk-G-D12, over the course of analysis yields 0.283049 ± 18 (2 sigma, *n* = 27), which is indistinguishable from our previously reported value determined by TIMS (0.283046 ± 16, 2 sigma, *n* = 9; [*Nowell et al.*, 1998]) and the previously reported value determined by PIMMS [*Kempton et al.*, 2000]. The data are corrected for mass fractionation during the run by normalization to ¹⁷⁹Hf/¹⁷⁷Hf of 0.7325 and are reported relative to

an accepted value of JMC 475 of 0.282160, as recommended by *Nowell et al.* [1998].

[73] The Nd, Hf, and some Sr analyses reported in Table 1 are averages of two or more analyses. In most cases, the duplicates represent repeat runs on the mass spectrometer using the same sample dissolution. In a few cases, new dissolutions were prepared. No discernible difference in Nd or Hf isotope values was noted for different dissolutions; Sr isotope analyses agreed less well (maximum difference = 85 ppm), which probably reflects variable removal of alteration products during leaching.

Acknowledgments

[74] Discussions with Andy Saunders and Doug Pyle provided useful insights into models for the origin of Indian MORB and the AAD. Thanks to David Wright for producing the software to perform the discriminant analysis at the last minute and to Bruce Charlier for his assistance completing those last few isotope analyses on the P54. Constructive comments by Roberta Rudnick, Bill White, and two anonymous reviewers significantly improved the paper. This research used samples and/or data provided by the Ocean Drilling Program (ODP). ODP is sponsored by the U.S. National Science Foundation (NSF) and participating countries under management of Joint Oceanographic Institutions (JOI), Inc. Funding for this research was provided by NERC grant GST/02/2792. This is NIGL publication #498.

References

- Alvarez, W., Geological evidence for the plate driving mechanism: The continental undertow hypothesis and the Australian-Antarctic Discordance, *Tectonics*, *87*, 6697–6710, 1990.
- Anderson, R. N., D. J. Spariousu, J. K. Weissel, and D. E. Hayes, The interrelation between variations in magnetic anomaly amplitudes and basalt magnetization and chemistry along the Southeast Indian Ridge, *J. Geophys. Res.*, *85*, 3883–3898, 1980.
- Arculus, R. J., Origin of the continental crust, *J. Proc. R. Soc. New South Wales*, *132*, 83–110, 1999.
- Barling, J., S. L. Goldstein, and I. A. Nicholls, Geochemistry of Heard Island (Southern Indian Ocean)—Characterization of an enriched mantle component and implications for enrichment of the sub-Indian-Ocean mantle, *J. Petrol.*, *35*, 1017–1053, 1994.
- Ben Othman, D., W. M. White, and J. Patchett, The geochemistry of marine sediments, island arc magma genesis and crust-mantle recycling, *Earth Planet. Sci. Lett.*, *94*, 1–21, 1989.
- Chauvel, C., and J. Blichert-Toft, A hafnium isotope and trace element perspective on melting of the depleted mantle, *Earth Planet. Sci. Lett.*, in press, 2002.

- Christie, D. M., B. P. West, D. G. Pyle, and B. Hanan, Chaotic topography, mantle flow and mantle migration in the Australian-Antarctic Discordance, *Nature*, 394, 637–644, 1998.
- Christie, D. M., et al., *Proceedings of the Ocean Drilling Program, Initial Reports*, vol. 187 [CD-ROM], Ocean Drill. Prog., College Station, Tex., 2001.
- Donnelly, K., C. H. Langmuir, S. L. Goldstein, and A. Lagatta, The origin of alkali and ocean island basalts: contradictions and solutions, *EOS Trans. AGU*, 82(47), F1402, Fall Meet. Suppl., 2001.
- Dosso, L., H. Bougault, P. Beuzart, J.-Y. Calvez, and J.-L. Joron, The geochemical structure of the South-East Indian Ridge, *Earth Planet. Sci. Lett.*, 88, 47–59, 1988.
- Fitton, J. G., A. D. Saunders, L. M. Larsen, B. S. Hardarson, and M. J. Norry, Volcanic rocks from the southeast Greenland margin at 63°N: composition, petrogenesis, and mantle sources, *Proc. Ocean Drill. Prog. Sci. Results*, 152, 331–350, 1998.
- Fitzsimons, I. C. W., A review of tectonic events in the East Antarctic Shield and their implications for Gondwana and earlier supercontinents, *J. African Earth Sci.*, 31, 3–23, 2000.
- Forsyth, D. W., R. L. Ehrenbard, and S. Chapin, Anomalous upper mantle beneath the Australian-Antarctic discordance, *Earth Planet. Sci. Lett.*, 84, 471–478, 1987.
- Frey, F. A., and D. Weis, Temporal evolution of the Kerguelen plume: geochemical evidence from ~38 to 82 Ma lavas forming the Ninetyeast Ridge, *Contributions to Mineralogy and Petrology*, 121, 12–28, 1995.
- Frey, F. A., N. J. McNaughton, D. R. Nelson, J. R. deLaeter, and R. A. Duncan, Petrogenesis of the Bunbury Basalt, Western Australia: interaction between the Kerguelen plume and Gondwana lithosphere, *Earth Planet. Sci. Lett.*, 144, 163–183, 1996.
- Galer, S. J. G., W. Abouchami, and J. D. Macdougall, Pb isotopic evidence for coherent mantle domains beneath the East Pacific Rise, *J. Conf. Abstr.*, 5(2), 421, 2000.
- Graham, D. W., J. E. Lupton, F. J. Spear, and D. M. Christie, Upper-mantle dynamics revealed by helium isotope variations along the southeast Indian ridge, *Nature*, 409, 701–703, 2001.
- Gurnis, M., R. D. Muller, and L. Moresi, Cretaceous vertical motion of Australia and the Australian-Antarctic Discordance, *Science*, 279, 1499–1504, 1998.
- Hamelin B., and C. J. Allègre, Large-scale regional units in the depleted upper mantle revealed by an isotope study of the South-West Indian Ridge, *Nature*, 315, 196–199, 1985.
- Hanan, B., D. G. Pyle, J. Blichert-Toft, D. M. Christie, and F. Albarede, Ultra-depleted hafnium isotopes from Australian-Antarctic Discordance MORB, *J. Conf. Abstr.*, 5(2), 478, 2000.
- Hart, S. R., A large scale isotope anomaly in the southern hemisphere mantle, *Nature*, 309, 753–757, 1984.
- Hemming, S. R., and S. M. McLennan, Pb isotope compositions of modern deep sea turbidites, *Earth Planet. Sci. Lett.*, 184, 489–503, 2001.
- Hochstaedter, A., J. Gill, R. Peters, P. Broughton, and P. Holden, Across-arc geochemical trends in the Izu-Bonin arc: Contributions from the subducting slab, *Geochemistry, Geophysics, Geosystems*, 2, Paper number 2000GC000105, 2001.
- Kelly, K., T. Plank, L. Farr, J. Ludden, H. Staudigel, and J. Alt, Subduction cycling of U, Th and Pb: perspectives from altered oceanic crust, *J. Conf. Abstr.*, 6, 384, 2001.
- Kempton P. D., Common Pb chemical procedures for silicate rocks and minerals, methods of data correction and an assessment of data quality at the NERC Isotope Geosciences Laboratory, *NIGL Rep. Ser. 78*, 26 pp., NERC Isotope Geosci. Lab., Keyworth, U.K., 1995.
- Kempton, P. D., G. M. Nowell, J. G. Fitton, A. D. Saunders, and R. N. Taylor, The Iceland plume in space and time: A Sr-Nd-Pb-Hf study of the North Atlantic rifted margin, *Earth Planet. Sci. Lett.*, 177, 255–271, 2000.
- Kempton P. D., G. M. Nowell, and T. L. Barry, Procedure for the High Precision Isotopic Analysis of Hafnium in silicate rocks and minerals by Plasma Ionisation Multi-collector Mass Spectrometry (PIMMS) and an Assessment of Data Quality at the NERC Isotope Geosciences Laboratory, *NIGL Rep. Ser. 171*, NERC Isotope Geosci. Lab., Keyworth, U.K., 2001a.
- Kempton, P. D., J. A. Pearce, J. Gill, and T. L. Barry, Mantle domain boundaries in the Western Pacific: Evidence from Nd-Hf Isotope Systematics, *J. Conf. Abstr.*, 6, 418, 2001b.
- Kent, R. W., A. D. Saunders, P. D. Kempton, and N. C. Ghose, Rajmahal basalts, Eastern India: mantle sources and melt distribution at a volcanic rifted margin, in *Large Igneous Provinces: Continental, Oceanic and Planetary Flood Volcanism*, *Geophys. Monogr. Ser.*, vol. 100, edited by J. J. Mahoney and M. F. Coffin, pp. 145–182, AGU, Washington, D.C., 1997.
- Klein, E. M., C. H. Langmuir, A. Zindler, H. Staudigel, and B. Hamelin, Isotope evidence of a mantle convection boundary at the Australian-Antarctic Discordance, *Nature*, 333, 623–629, 1988.
- Klein, E. M., C. H. Lagmuir, and H. Staudigel, Geochemistry of basalts from the Southeast Indian Ridge, *J. Geophys. Res.*, 96, 2089–2107, 1991.
- Kuo, B.-Y., Thermal anomalies beneath the Australian-Antarctic discordance, *Earth Planet. Sci. Lett.*, 119, 349–364, 1993.
- Lanyon R., R. Varnet, and A. J. Crawford, Tasmanian Tertiary basalts, the Balleny plume and opening of the Tasman Sea (southwest Pacific Ocean), *Geology*, 21, 555–558, 1993.
- Lanyon, R., A. J. Crawford, and S. M. Eggins, Westward migration of Pacific Ocean upper mantle into the southern Ocean region between Australia and Antarctica, *Geology*, 23, 511–514, 1995.
- Mahoney J. J., A. P. le Roex, Z. Peng, R. L. Fisher, and J. H. Natland, Southwestern limits of the Indian Ocean Ridge mantle and the origin of low ²⁰⁶Pb/²⁰⁴Pb mid-ocean ridge basalts: isotope systematics of the central Southwest Indian Ridge (17°–50°E), *J. Geophys. Res.*, 97, 19771–19790, 1992.
- Mahoney, J. J., W. B. Jones, F. A. Frey, V. J. M. Salters, D. G. Pyle, and H. L. Davies, Geochemical characteristics of lavas from Broken Ridge, the Naturaliste Plateau and southernmost Kerguelen Plateau: Cretaceous plateau volcanism in the southeast Indian Ocean, *Chemical Geology*, 120, 315–345, 1995.

- Mahoney, J. J., W. M. White, B. G. J. Upton, C. R. Neal, and R. A. Scrutton, Beyond EM-1: Lavas from Afanasy-Nikitin Rise and the Crozet Archipelago, Indian Ocean, *Geology*, *24*, 615–618, 1996.
- Mahoney, J. J., R. Frei, M. L. G. Tejada, X. X. Mo, P. T. Leat, and T. F. Nägler, Tracing the Indian Ocean Mantle domain through time: isotopic results from old west Indian, east Tethyan and south Pacific seafloor, *J. Petrol.*, *39*, 1285–1306, 1998.
- Marks, K. M., P. R. Vogt, and S. A. Hall, Residual depth anomalies and the origin of the Australian-Antarctic Discordance zone, *J. Geophys. Res.*, *95*, 17325–17337, 1990.
- Marks, K. M., D. T. Sandwell, P. R. Vogt, and S. A. Hall, Mantle downwelling beneath the Australian-Antarctic discordance zone: Evidence from geoid height versus topography, *Earth Planet. Sci. Lett.*, *103*, 325–338, 1991.
- Marsh, J. G., A. C. Brenner, B. D. Beckley, and T. V. Martin, Global mean sea surface based upon the Seasat altimeter data, *J. Geophys. Res.*, *91*, 3501–3506, 1986.
- Michard, A., R. Montigny, and R. Schlich, Geochemistry of the mantle beneath the Rodriguez Triple Junction and the South-East Indian Ridge, *Earth Planet. Sci. Lett.*, *78*, 104–114, 1986.
- Nowell, G. M., P. D. Kempton, J. G. Fitton, A. D. Saunders, and R. Taylor, High precision Hf isotope measurements of MORB and OIB by thermal ionisation mass spectrometry: Insights into the depleted mantle, *Chem. Geol.*, *149*, 211–233, 1998.
- Palmer, J., J.-C. Sempéré, D. M. Christie, and J. Phipps Morgan, Morphology and Tectonics of the Australian-Antarctic discordance between 123° and 128°E, *Mar. Geophys. Res.*, *15*, 121–152, 1993.
- Patchett, P. J., Importance of Lu-Hf isotopic system in studies of planetary chronology and chemical evolution, *Geochim. Cosmochim. Acta*, *47*, 81–91, 1983.
- Patchett, P. J., W. M. White, H. Feldmann, S. Kielinczuk, and A. W. Hofmann, Hafnium/rare earth element fractionation in the sedimentary system and crustal recycling into the Earth's mantle, *Earth Planet. Sci. Lett.*, *69*, 365–378, 1984.
- Pearce, J. A., and P. D. Kempton, Petrogenetic significance of Hf isotope variations in Island Arcs, *J. Conf. Abstr.*, *6*, 385, 2001.
- Pearce, J. A., and D. W. Peate, Tectonic implications of the composition of volcanic arc magmas, *Annu. Rev. Earth Planet. Sci.*, *23*, 251–285, 1995.
- Pearce, J. A., P. E. Baker, P. K. Harvey, and I. W. Luff, Geochemical evidence for subduction fluxes, mantle melting and fractional crystallisation beneath the South Sandwich island arc, *J. Petrol.*, *36*, 1073–1109, 1995.
- Pearce, J. A., P. D. Kempton, G. M. Nowell, and S. R. Noble, Hf-Nd element and isotope perspective on the nature and provenance of mantle and subduction components in arc-basin systems: examples from the western Pacific, *J. Petrol.*, *40*, 1579–1612, 1999.
- Peate, D. W., T. F. Kokfelt, C. J. Hawkesworth, P. W. van Calsteren, J. M. Hergt, and J. A. Pearce, U-series isotope data on Lau Basin Glasses: the role of subduction-related fluids during melt generation in back-arc basins, *J. Petrol.*, *42*, 1449–1470, 2001.
- Plank, T., and C. H. Langmuir, The chemical composition of subducting sediment and its consequences for the crust and mantle, *Chem. Geol.*, *145*, 325–394, 1998.
- Pyle, D. G., D. M. Christie, and J. J. Mahoney, Resolving an isotopic boundary within the Australian-Antarctic Discordance, *Earth Planet. Sci. Lett.*, *112*, 161–178, 1992.
- Pyle, D. G., D. M. Christie, J. J. Mahoney, and R. A. Duncan, Geochemistry and geochronology of ancient southeast Indian and southwest Pacific seafloor, *J. Geophys. Res.*, *100*, 22,261–22,282, 1995.
- Pyle D. G., D. M. Christie, B. B. Hanan, R. B. Pedersen, and Shipboard Scientific Party, Regional isotopic constraints on eastern Indian and western Pacific MORB mantle components, *Eos Trans. AGU*, *81*(46), F1285, Fall Meet. Suppl., 2000.
- Rehkämper, M., and A. W. Hofmann, Recycled ocean crust and sediment in Indian Ocean MORB, *Earth Planet. Sci. Lett.*, *147*, 93–106, 1997.
- Royer, J.-Y., and D. T. Sandwell, Evolution of the Eastern Indian Ocean since the Late Cretaceous: constraints from Geosat altimetry, *J. Geophys. Res.*, *94*, 13,755–13,782, 1989.
- Royse K. R., P. D. Kempton, and D. P. F. Darbyshire, Procedure for the analysis of rubidium-strontium and samarium-neodymium isotopes at the NERC Isotope Geosciences Laboratory, *NIGL Rep. Ser. 121*, 28 pp., NERC Isotope Geosci. Lab., Keyworth, U.K., 1998.
- Russo, C. J., et al., Ocean Drilling Program Leg 187 to the Australian-Antarctic Discordance: A major and trace element view of a 30 Ma Mantle boundary, *Eos Trans. American Geophysical Union*, *81*(46), F1285, Fall Meet. Suppl., 2000.
- Salters, V. J. M., The generation of mid-ocean ridge basalts from the Hf and Nd isotope perspective, *Earth Planet. Sci. Lett.*, *141*, 109–123, 1996.
- Salters, V. J. M., and W. M. White, Hf isotope constraints on mantle evolution, *Chem. Geol.*, *145*, 447–460, 1998.
- Sempéré J.-C., J. Palmer, D. M. Christie, J. Phipps Morgan, and A. N. Shor, Australian-Antarctic discordance, *Geology*, *19*, 429–432, 1991.
- Smith, W. H. F., and D. T. Sandwell, Global seafloor topography from satellite altimetry and ship depth soundings, *Science*, *277*, 1956–1962, 1997.
- Storey, M., A. D. Saunders, J. Tarney, I. L. Gibson, M. J. Norry, M. F. Thirlwall, P. Leat, R. N. Thompson, and M. A. Menzies, Contamination of the Indian Ocean asthenosphere by the Kerguelen-Heard mantle plume, *Nature*, *338*, 574–576, 1989.
- Sun, S. S., and W. F. McDonough, Chemical and isotopic systematics of oceanic basalts: implications for mantle composition and processes, in *Magmatism in the Ocean Basins*, edited by A. D. Saunders and M. J. Norry, *Geol. Soc. London Spec. Publ.*, *42*, 313–345, 1989.
- Todt, W., R. A. Cliff, A. Hanser, and A. W. Hofmann, Evaluation of a 202Pb-205Pb double spike for high-precision lead isotope analysis, in *Earth Processes: Reading the Isotope Code*, *Geophys. Monogr. Ser.*, vol. 95, edited by S. R. Hart and A. Basu, pp. 429–437, AGU, Washington, D.C., 1996.
- Unrug, R., The assembly of Gondwanaland, *Episodes*, *19*, 11–20, 1996.



- Vervoort, J. D., P. J. Patchett, J. J. Blichert-Toft, and F. Albarède, Relationships between Lu-Hf and Sm-Nd isotopic systems in the global sedimentary system, *Earth Planet. Sci. Lett.*, *168*, 79–99, 1999.
- Vlastelic, I., D. Aslanian, L. Dosso, H. Bougault, J. L. Olivet, and L. Geli, Large-scale chemical and thermal division of the Pacific mantle, *Nature*, *399*, 345–350, 1999.
- Vogt, P. R., N. Z. Cherkis and G. A. Morgan, Project Investigator-I: Evolution of the Australian-Antarctic Discordance from a detailed aeromagnetic study, in *Antarctic Earth Science: Proceedings 4th International Symposium on Antarctic Earth Science*, edited by R. L. Oliver, P. R. James, and J. Jago, Aust. Acad. of Sci., Canberra, 1984.
- Weis, D., F. A. Frey, H. Leyrit, and I. Gautier, Kerguelen archipelago revisited: Geochemical and isotopic study of the southeast province lavas, *Earth Planet. Sci. Lett.*, *118*, 101–119, 1993.
- Weissel, J. K., and D. E. Hayes, Asymmetric seafloor spreading south of Australia, *Nature*, *231*, 518–522, 1971.
- Weissel, J. K., and D. E. Hayes, The Australian-Antarctic Discordance: New results and implications, *J. Geophys. Res.*, *79*, 2579–2587, 1974.
- West, B. P., J.-C. Sempéré, D. G. Pyle, J. Phipps Morgan, and D. M. Christie, Evidence for variable upper mantle temperature and crustal thickness in and near the Australian-Antarctic Discordance, *Earth Planet. Sci. Lett.*, *128*, 135–153, 1994.
- Yang, H. J., F. A. Frey, D. Weis, A. Giret, D. Pyle, and G. Michon, Petrogenesis of the flood basalts forming the northern Kerguelen archipelago: Implications for the Kerguelen plume, *J. Petrol.*, *39*, 711–748, 1998.
- Zhang, M., S. Y. O'Reilly, and D. Chen, Location of Pacific and Indian mid-ocean ridge-type mantle in two time slices: Evidence from Pb, Sr, and Nd isotopes for Cenozoic Australian basalts, *Geology*, *27*, 39–42, 1999.